Strål
säkerhets
myndigheten
Swedish Radiation Safety Authority

Research

Estimates of J-integral and COD for circumferential through wall cracks under global bending including the effect of pipe end restraint

2020:16

Author: Daniel Mångård, Dave Hannes, Tobias Bolinder Kiwa Inspecta Technology AB, Solna
Report number: 2020:16
ISSN: 2000-0456
Available at: www.ssm.se

SSM perspective

Background

Leak-before-break (LBB) piping assessments have shown that piping systems can withstand long through-wall cracks before pipe rupture is expected. This is somewhat because pipe ends are restrained. In LBB assessments analyses are often performed for a pipe segment uncoupled from the piping system, as pipe ends are assumed unrestrained. This assumption is conservative for crack assessment. However, predictions of the crack opening displacement will be overestimated and hence the calculated leakage rate.

The present study aims to investigate what impacts the assumption degree of restraint at the ends of an analysed piping segment have on leak-before-break assessments and leakage rate calculations.

Results

The study conclude that crack opening displacements were influenced by restraint length, relative crack length, degree of restraint and material constitutive properties in the same way as the J-values. However, the relative difference was generally smaller for the crack opening displacement. The crack opening displacement values and subsequently the leak rates may be overestimated in leak-before-break assessments if pipe ends restraints are not carefully considered.

It is recommended that the influence from restraint is studied in detail as a leak-before-break assessment of a selected case based on a real piping system analysis. The results from a detailed simulation of loadings and structural stiffness should be compared with the results obtained from common practice methods. Reliable conclusions can only be drawn taking the margin against fracture, leak detection as well as degradation mechanisms into account.

Relevance

The work has increased the understanding for how the degree of restraint at the ends of an analysed piping segment will affect leak-before-break assessments and leakage rate calculations. The results can also lead to improved recommendations for how to perform analyses of cracked piping components

Need for further research

SSM have not identified any need of further research at the moment.

Project information

Contact person SSM: Fredrik Forsberg
Reference: SSM2016-563 / 7030046-00

Strål
säkerhets
myndigheten
Swedish Radiation Safety Authority

Author: Daniel Mångård, Dave Hannes, Tobias Bolinder

Kiwa Inspecta Technology AB, Solna

2020:16

Estimates of J-integral and COD for circumferential through wall cracks under global bending including the effect of pipe end restraint

Date: December 2020
Report number: 2020:16 **ISSN:** 2000-0456
Available at www.stralsakerhetsmyndigheten.se

This report concerns a study which has been conducted for the Swedish Radiation Safety Authority, SSM. The conclusions and viewpoints presented in the report are those of the author/authors and do not necessarily coincide with those of the SSM.

Sammanfattning

Analys av läckage före brott hos rörledningar utvärderar förhållandet mellan läckageflöden och begränsande faktorer såsom brott och plastisk kollaps. Det förväntas att dessa i okänd grad kan påverkas av inspänningen vid ändarna av ett analyserat rörsegment.

Denna rapport redovisar en undersökning av inspänningens inverkan på *J*-integralen och spricköppning för ett flertal olika kombinationer av genombrytande omkretssprickor i rörsegment och global böjning.

Den linjärt elastiska såväl som elastisk-plastiska *J*-integralen visade en betydande variation längs de analyserade sprickfronterna och det kan vara nödvändigt att diskutera tillämpning och relevans för användningen av idealiserade genombrytande omkretssprickor.

Efter den elastiska fasen ökade den elastisk-plastiska *J*-integralen främst utmed den inre delen av sprickfronten. Marginalen mot brott utifrån en elastisk-plastisk analys har därför utvärderats med hänsyn till tillståndet längs den inre delen av sprickfronten, i motsats till R6-utvärderingen med plastisk korrigering baserat på den linjärt elastiska *J*-integralen vid sprickfrontens ytbrytande punkter.

Spricköppningen påverkades av rörsegments längd, relativ spricklängd, inspänningsgrad och materialegenskaper på samma sätt som *J*-integralen. Den relativa skillnaden var generellt mindre för spricköppningen. Spricköppningen och därmed läckflöden kan riskera att överskattas vid bedömningar av läckage före brott om inspänningen vid ändarna av ett analyserat rörsegment inte beaktas.

Det rekommenderas att inverkan från inspänning studeras i detalj genom analys av läckage före brott för ett utvalt fall från en analys av ett verkligt rörsystem. Resultat från en detaljerad simulering som beaktar faktiska belastningar och strukturell styvhet bör jämföras mot resultat från vanliga metoder. Säkra slutsatser kräver att marginalen mot brott, läckagedetektering samt skademekanismer beaktas.

Summary

Leak-before-break piping assessments evaluate the relationship between leakage rates and limiting factors such as fracture and plastic collapse. It is expected that these may be influenced to an unknown degree by the restraint at the ends of an analysed piping segment.

The present work has examined the effect from pipe end restraint on the *J*-integral and crack opening displacement for a variety of combinations of circumferential through-wall cracks in piping segments under global bending.

Linear elastic as well as elastic-plastic *J*-values varied significantly along the analysed crack fronts such that it may be necessary to discuss the applicability and relevance of idealised circumferential through-wall cracks.

Furthermore, the elastic-plastic *J*-values increased primarily along the interior part of the crack front after the elastic phase. The margin against fracture based on an elastic-plastic analysis was therefore determined by the state along the interior part of the crack front, in contrast to the R6-estimation with plastic correction of linear elastic *J*-values determined at the surface breaking points.

Crack opening displacements were influenced by restraint length, relative crack length, degree of restraint and material constitutive properties in the same way as the *J*-values. However, the relative difference was generally smaller for the crack opening displacement. The crack opening displacement values and subsequently the leak rates may be overestimated in leak-before-break assessments if pipe end restraints are not carefully considered.

It is recommended that the influence from end restraint is studied in detail as a leak-before-break assessment of a selected case based on a real piping system analysis. The results from a detailed simulation of loadings and structural stiffness should be compared with the results obtained from common practice methods. Reliable conclusions can only be drawn taking the margin against fracture, leak detection as well as degradation mechanisms into account.

Table of content ***Page***

1 INTRODUCTION

1.1 Background

A leak-before-break (LBB) piping evaluation is usually preceded by a piping system analysis. The piping system analysis may be static or dynamic with globally and locally declared loads along with rigid and flexible restraints and is usually evaluated assuming linearly elastic material behaviour. Resulting structural stresses, forces and moments can be extracted at selected locations to serve as input for e.g. LBB analyses. LBB analyses are often performed on limited piping segments judged representative to the location within the actual piping system. These analyses are often based on standard geometries, which in the case of a pipe segment likely involves unrestrained pipe ends. The use of such standard geometries is a common and established approximation but may potentially deviate from the actual restraint imposed from the piping system. Restraint can occur in many forms, from pipe bends and curves to hinges and supports, all of which influence the degree of restraint and the restraint length. It can be difficult to estimate the potential deviation without a detailed analysis, for instance when the analysed pipe segment is uncoupled from the piping system.

When a propagating surface crack has initiated in a pipe wall, it may either grow into a stable through-wall crack (TWC) or become unstable before wall penetration resulting in rapid and sudden crack propagation. For the latter case a double-ended guillotine break (DEGB) is then usually the assumed result of failure. The sudden failure of the piping prevents early intervention to avoid the potentially catastrophic consequences. However, leakage may occur prior to final rupture (i.e. LBB) in the case of a stable TWC. In this case, early detection of leakage allows execution of preventive measures to avoid sudden rupture of the piping and detection of unsuspected damage to the piping component. LBB design has therefore an important role in pressure vessel and piping design. More information on the background of LBB and different assessment procedures mainly used in the nuclear industry are discussed in [1].

The LBB procedures are based on end-capped pipe models allowing free rotation of the pipe ends. The resulting predictions will overestimate the crack opening displacement (COD), as in reality the piping system will act as a restraint and prevent to a certain extent free rotation. Consequently, the resulting predicted leakage rates will be overestimated, which is detrimental to the LBB approach. Realistic leakage rates will be smaller than the predictions and may potentially be less than a minimum leakage rate detection limit inducing failure of the LBB design. Contrary to the non-conservative COD predictions, the pipe model allowing free rotation will yield larger internal bending moments than those prevailing in a cracked pipe section of the piping system. Crack driving forces related to the bending moment will thus

be conservative for a circumferential TWC. As a result, actual critical crack lengths will be larger than the predictions in the LBB analysis. It is thus not evident how the overall conservatism of the LBB procedure may be affected by neglecting the restraint effect.

The effects of a restraint on failure were first highlighted during the International Piping Integrity Research Group (IPIRG) program [2]. The investigation consisted of unique realistic experiments on 16-inch diameter schedule 100 pipes with various flaws and subjected to both PWR conditions and a combination of inertial and seismic loads. An unexpected degree of stability in the pipe-system experiments was observed, as only two experiments resulted in DEGB and only after extensive crack growth. The crack lengths were indeed about 95% of the circumference prior to the final failure event, see Figure 1. The critical flaw size of short pipe sections subjected to the applied pressure loading was however estimated to about 65 % of the circumference based on a net section collapse analysis assuming free rotation of the pipe ends. The discrepancy suggested that the restraint of the remaining piping system prevented free rotation of the flawed pipe section ends when subjected to internal pressure. The restraint then effectively reduced the applied bending moment due to pressure induced bending (PIB), see Figure 2. As such an increase of load bearing capacity of the cracked pipe was obtained, which resulted in increased critical flaw sizes for pressure loading [2, 3].

The effect of restraint of pressure induced bending on LBB was included in the investigation performed in NUREG/CR-6443 [4]. The effect was found to be of high significance for small diameter piping but considered negligible for large diameters. NUREG/CR-6300 [5] performed an elastic study to evaluate the restraint effect of PIB on the COD. The effect was found small for small crack sizes, but significant for larger crack sizes, especially in combination with small diameters. Indeed, the leakage crack size for a smaller pipe will correspond to a larger portion of the pipe circumference, hence the pressure induced bending will be larger for smaller piping with free ends. As a result, the effect of a restraint will more strongly affect the COD when compared to a large diameter piping. Based on these previous studies the development of a technical basis for LBB evaluation procedures reported in NUREG/CR-6765 [6] highlights that the flexibility of the piping system should be considered in the boundary conditions for the determination of COD for the leakage rate computations, as restraint of pressure induced bending on the COD is expected to be an influencing factor in leakage crack size predictions.

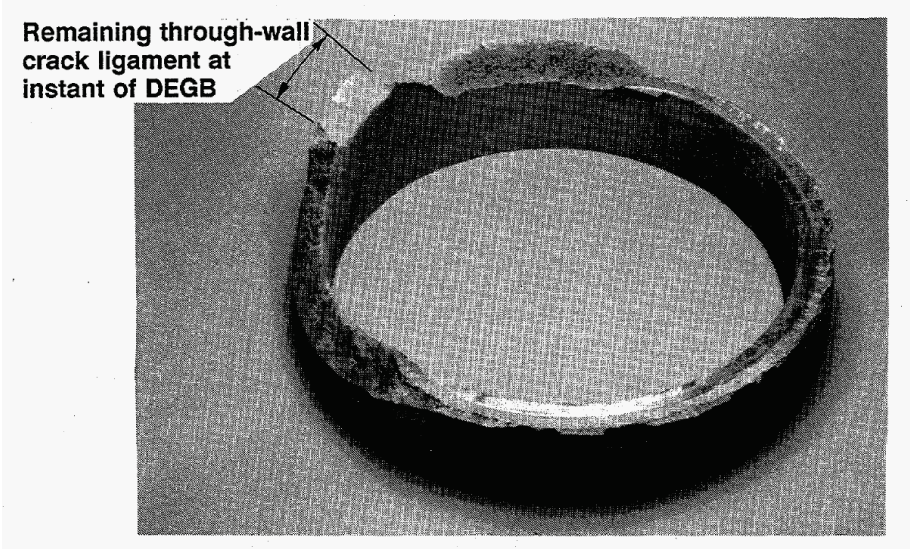

Figure 1 Photograph of the fracture surface from a double-edged guillotine break [2].

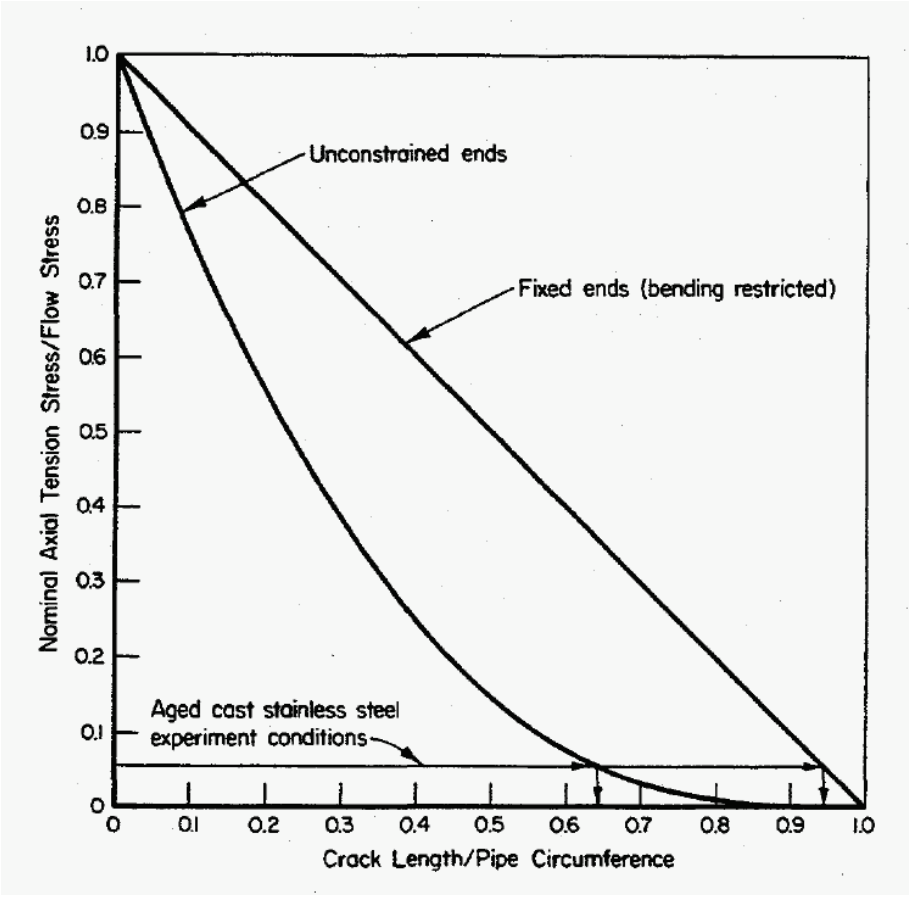

Figure 2 Net section collapse analyses predictions as function of relative crack size [2].

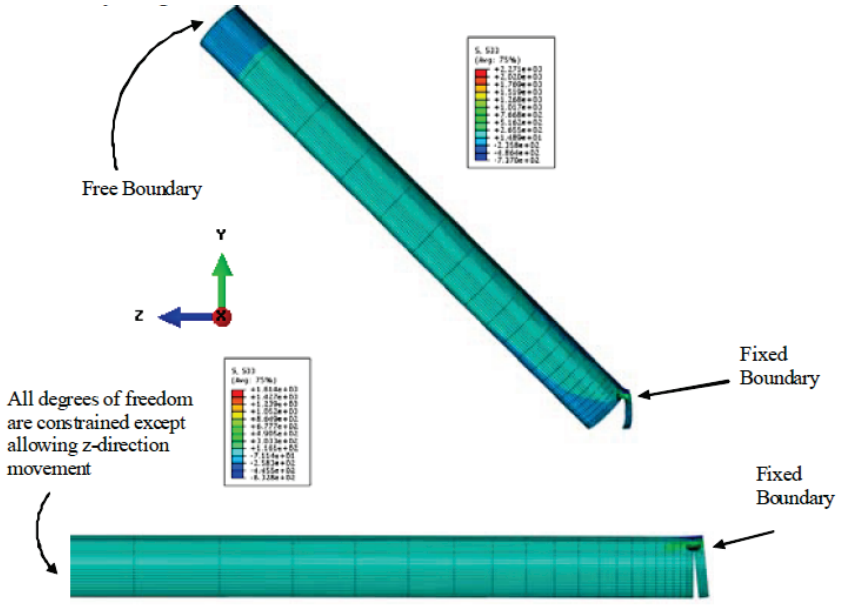

Figure 3 Example FE-model with different restraint and pressure induced bending [3].

FE modelling of a cracked pipe section in [3] reported indeed large rotations for large crack sizes, which was considered unrealistic due to exiting restraints introduced by pump nozzles, the RPV, etc. present in the piping system, see Figure 3. The fixed-end condition gives much smaller COD but was not considered to be representative of the piping system. Therefore, the pipe model was introduced in a larger pipe system model following the recommendations in [6] and resulting in realistic restraints, which induced a significant reduction of leak rates. The work in [3] also modelled the piping system with special cracked-pipe elements, which were validated against full 3D cracked-pipe sections and obtained results consistent with experimental DEGB results in [2].

The study of the restraint effect was also included in the Batelle Integrity of Nuclear Piping (BINP) Program [7], but concluded that the restraint effect is a minor issue for LBB analyses. It is expected to play a role only for small diameter pipes for which the leakage crack length is a large percentage of the pipe circumference (near 50%). Previous investigations assumed linear elastic material behaviour, but a more recent study by Kim [8] considered elastic-plastic material behaviour. The restraint effect of PIB on the elastic-plastic COD was found more significant than for linear elastic analyses.

More recent research has focused on quantifying the effect of restraint on the COD using correction factors. These research efforts aimed at the removal or reduction of a source for non-conservatism in the LBB evaluation procedure. SKI 2005/83 [9] refers for instance to work by Olson et al. [10] on quantitative correction factors to account for the effects of PIB on COD predictions. The work considers asymmetric

restraints which are more representative for the conditions in piping systems. Analytical expressions are derived based on the concept of restraint length and were obtained by curve fitting to FE results. The restraint length is defined as the distance from the cracked pipe section to a fixed section. Young and Olson [11] continued the work on restraint effects on COD based on an alternative rotational stiffness approach, which requires the local system stiffness to modify or correct the unrestrained COD. Alternative analytical solutions for the COD based on the concept of restraint length and including the effects of plastic deformation have been derived by Kim [12, 13]. More recently Kim et al. [14] also proposed a method to correct the COD based on an effective applied moment. The main research effort in the topic of the restraint effect has been on the source for non-conservatism, i.e. the over-estimation of the COD, and not on reducing or estimating the conservatism of crack driving forces used during the LBB evaluation. Some work in this direction was initiated by Kim et al. [15]. The overall conservatism of an LBB analysis was quantified by investigating the conservatism of the applied moment. A considerable decrease in the applied moment was observed due to considering nonlinear material behaviour and effects related to the presence of a crack.

Numerical modelling of a cracked pipe segment to investigate the restraint effect has considered different piping geometries typically defined by combinations of the outer or mean diameter and the ratio of the mean radius over the wall thickness. A frequently used value of the mean pipe radius over wall thickness in investigations was equal to 10, see [4, 5, 14, 8]. Other investigations [10, 11, 12, 13] (sometimes partially) used the set {2, 5, 10, 20, 40}. Realistic values seem however to be included in the range 4 – 7, see [7, 3, 10]. The outer or mean pipe diameter, when reported, was then generally taken equal to one of the following values: 114.3, 323.9 or 711.2 mm characterizing respectively small, intermediate and large piping. The TWC dimension was usually expressed in terms of the normalized crack length (normalized crack angle) consisting of the ratio of the crack length over the pipe circumference. Several numerical studies [4, 5, 10, 12, 8, 13, 14] have (sometimes partially) used the set {1/8, 1/4, 1/2} as normalized crack length. An alternative set equal to {0.05, 0.1, 0.25, 0.5, 0.75, 0.9} was used in [11]. For the studies using the concept of restraint length, restraint lengths normalized either by the outer or mean pipe diameter were reported. The set of normalized restraint lengths {1, 5, 10, 20} was recurrently used in several numerical investigations [4, 5, 10, 12, 8, 13, 14]. Realistic applications can however present normalized restraint lengths ranging from about 0.1 to more than 100, see the PWR piping system reported in [10].

1.2 Aims and objectives

LBB assessments of detected and postulated flaws evaluate the relationship between leakage rates and limiting factors such as fracture and plastic collapse. It is expected that these may be influenced to an unknown degree by the restraint at the pipe ends.

The present work examines the effect from restraint on the *J*-integral and COD for a variety of combinations of geometry and boundary conditions for linear elastic as well as elastic-plastic material behaviour. Each combination of unrestrained pipe ends and linear elastic material behaviour is considered as a reference case for the evaluation.

2 NUMERICAL ANALYSES

2.1 Geometry and boundary conditions

The current work was carried out for straight pipes with two dimensions R_m = 50 and 300 mm, radius to thickness ratio R_m/t = 10 and three normalized restraint lengths L/D_m = 5, 10 and 20.

Circumferential TWCs with lengths corresponding to θ/π = 1/8, 1/4 and 1/2 were inserted at the pipe mid-length for each pipe geometry, see Figure 4. Each TWC was positioned at the location with maximum tensile bending stress.

The boundary conditions applied to each geometry were designed to achieve different restraints at the pipe ends but identical nominal bending stress at the mid-length cross section. Applying bending moments at the pipe ends is a simple way to accomplish global bending but requires otherwise unrestrained pipe ends. Restraining the pipe ends therefore requires an alternative loading. Concentrated loads and restraints near the pipe mid-length were considered unacceptable to avoid undesirable influence on the results within the crack plane proximity. The solution was to apply a vertical acceleration along the length of the pipe. This resulted in the three boundary conditions denoted BC1, BC2 and BC3 in Figure 5.

BC1 corresponds to the reference case with bending moment applied at otherwise free pipe ends. The bending moment was replaced by a distributed vertical load in BC2. BC3 is identical to BC2 apart from the prevented rotation at the pipe ends.

2.2 Material data

The analyses in this report have been performed assuming a ferritic low-alloy steel which can be found in nuclear piping systems. The material was modelled as linear elastic as well as elastic-plastic. The fracture toughness was K_{Ic} = 220 MPa$\sqrt{m}$ (J_{Ic} = 215 kN/m). The linear elastic material was represented by a Young's modulus E=205 GPa and a Poisson's ratio ν=0.3. The elastic-plastic material with a yield stress σ_y=500 MPa and ultimate tensile strength σ_u=1000 MPa was modelled with a von Mises behaviour and isotropic hardening following the stress-strain curve depicted in Figure 6.

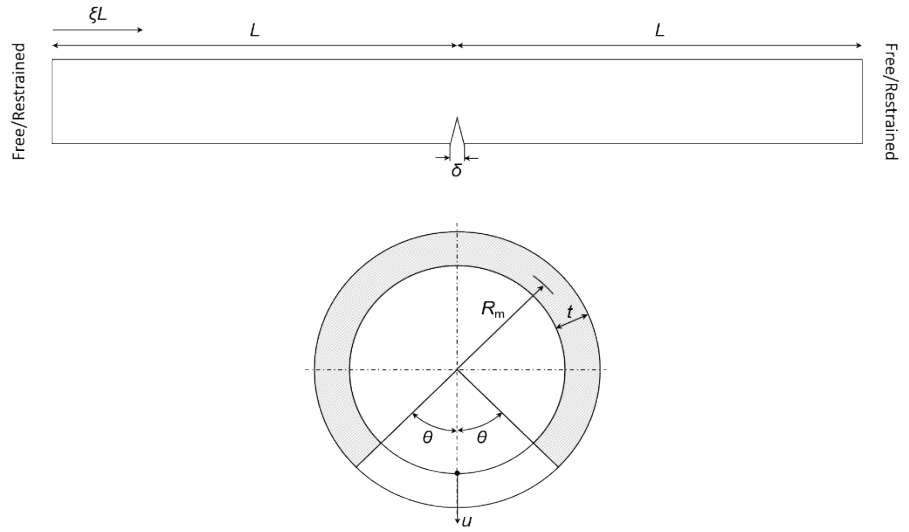

Figure 4 A circumferential TWC at the pipe mid-length.

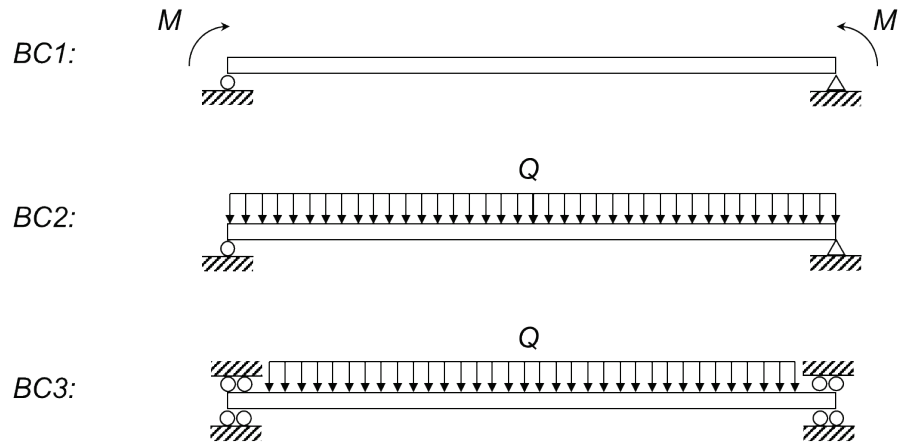

Figure 5 The three boundary conditions denoted BC1, BC2 and BC3.

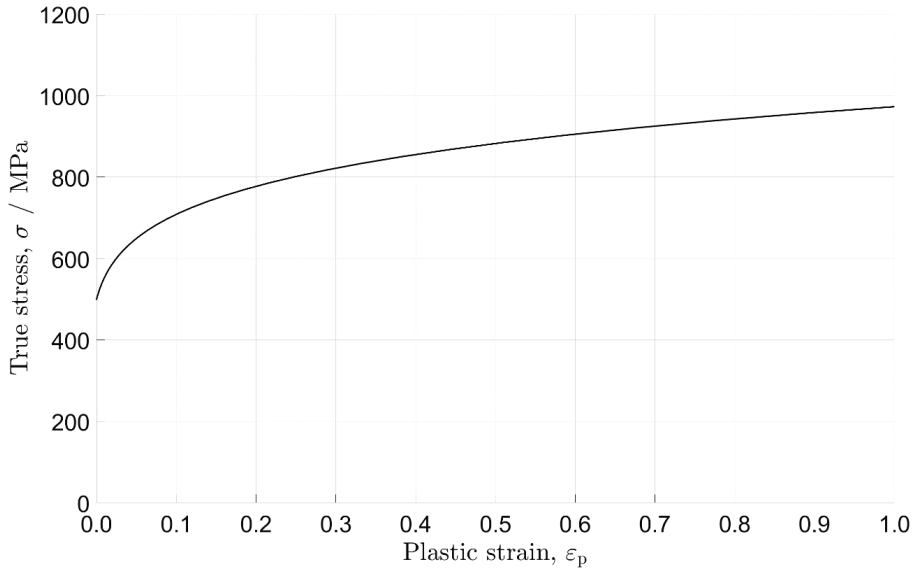

Figure 6 Stress-strain curve for the elastic-plastic material.

2.3 FE-model

Because of symmetry, only one quarter of the pipes were considered in the FE-modelling. Linear elastic and elastic-plastic small strain analyses were performed in Abaqus [16] with meshes of tri-quadratic 20-node solid elements with reduced integration. The mesh in the integration domain along the crack front was organised in a focused spider web arrangement, see Figure 7. A finite radius is advised at the crack tip for large strain analyses but was judged unnecessary due to the selection of small strain analysis. The crack tip was instead modelled as initially sharp with tied and untied crack front nodes for the linear elastic analyses and elastic-plastic analyses, respectively. The radius of the integration domain along the crack front was equal to the pipe thickness.

The element density along the crack front was judged enough with 10 elements in the thickness direction, 12 elements in the circumferential direction (15° angle) and 10 elements in the radial direction. Apart from the initially sharp crack tip, it was ensured that no element in the models had aspect ratios below 1/100. The 10 element segments in the thickness direction resulted in 21 equidistant evaluation points along each crack front.

Horizontal symmetry conditions were applied at the crack plane for the remaining ligament. The models were vertically anchored at a reference point connected to the surface of the pipe end. The connection between the reference point and the surface of the pipe end were either distributed coupling constraints for BC1 or kinematic coupling constraints for BC2 and BC3.

The case of high restraint at the pipe ends resulted in stress concentrations with yielding at low load factors. This was an unwanted artefact that needed to be solved to avoid any influence on the results in the crack vicinity. It was avoided by assigning two material regions, see Figure 7. Half of the restraint length (closest to the restraint) was always modelled as linear elastic while the other half of the restraint length (closest to the crack plane) was modelled as either linear elastic or elastic-plastic, depending on the analysis.

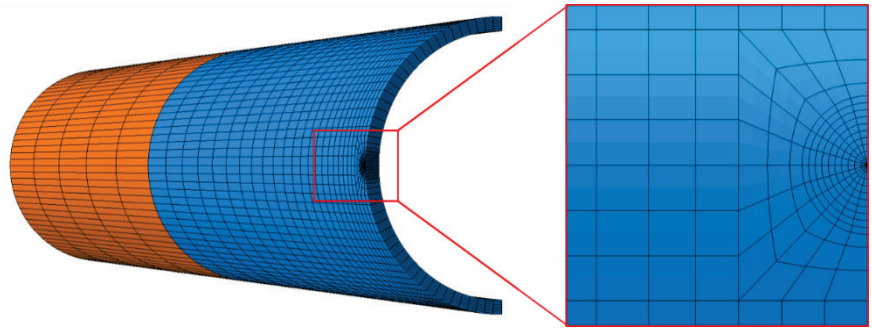

Figure 7 The FE-model with two material regions and crack tip.

2.4 Verification of the FE- model

Verification of the FE-model was carried out in several consecutive steps with the purpose of verifying evaluations of *J*-integrals and CODs. Each step was intended to confirm different characteristics of the FE-model.

The first step was to ensure that each combination of constraint and load were correctly applied and result in identical nominal bending stress at the cross section of the prospective crack plane. The maximum bending stress was evaluated for each nominal geometry and combination of restraint and load. Classical beam theory may be used as reference since shear deformation is expected to be negligible for unrestrained pipe ends and sufficiently long pipes. Normalized deflection (transverse displacement) versus normalized pipe length coordinate for three different boundary conditions and two different restraint lengths are shown in Figure 8 and Figure 9. The discrepancies in Figure 8 show that the normalized pipe length L/D_m=5 was not sufficiently long to make the shear deformation for BC2 and BC3 negligible.

Normalized global bending stress versus normalized pipe length coordinate for three different boundary conditions and restraint lengths are shown in Figure 10.

Computation of the *J*-integral was carried out at 21 equidistant points (10 element segments) along the crack front for two reference cases with a linear elastic material. Results at each point along the crack front were determined based on the average value from integration contours 5 to 8 (i.e. excluding the four innermost and two outermost contours). K_I-values were computed from the average *J*-integral values using the plane strain formulation $K_I = \sqrt{JE/(1-\nu^2)}$. Normalized stress intensity factor values were verified against reference solutions published in [17]. The current analyses were carried out for geometries based on R_m/t = 10 while the reference is based on R_i/t = 10. A correction of the applied bending stress was undertaken to account for the difference in geometry. The current results and the reference values are in good agreement, see Figure 11.

Values close to the free surface deviate which is explained by different methods to account for the weaker singularity at the free surface. Reference [17] suggests fitting the stress intensity factors to a fourth-degree polynomial, excluding the first and last two points (first and last element segment) along the crack front. The values close to the free surface can then be updated based on the resulting curve fit in the corresponding region. This approach was used in the current postprocessing procedure and applied to all computations carried out within this report.

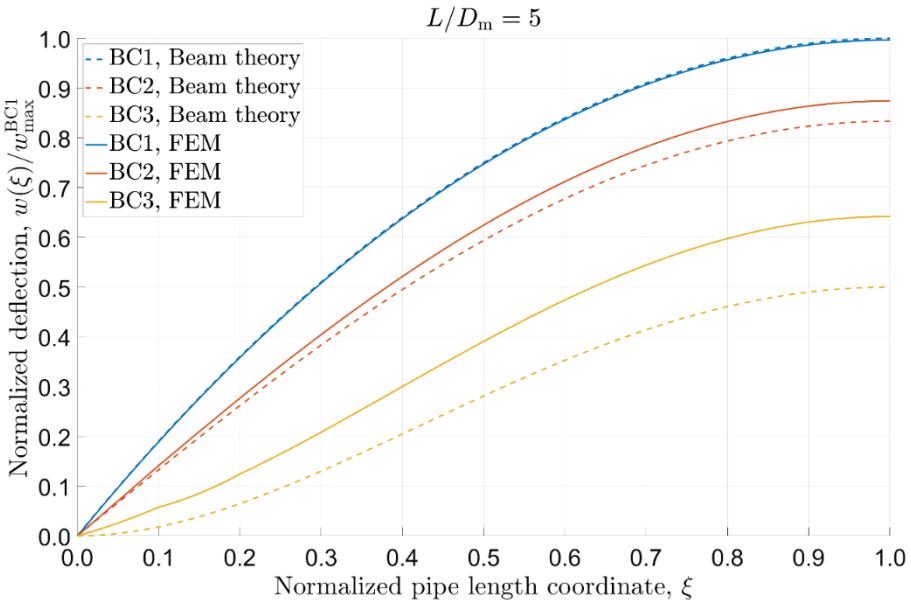

Figure 8 Normalized deflection versus normalized pipe length coordinate for L/D_m=5.

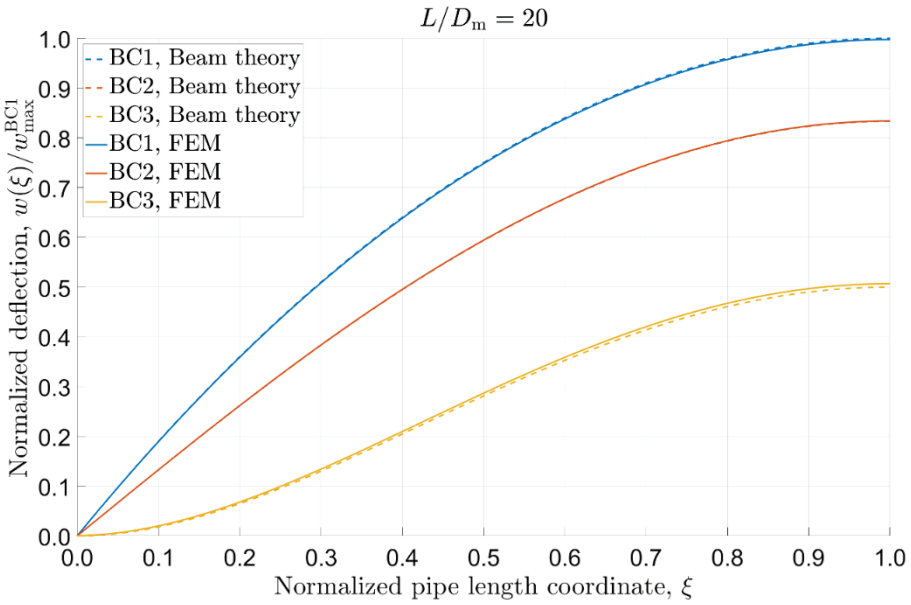

Figure 9 Normalized deflection versus normalized pipe length coordinate for L/D_m=20.

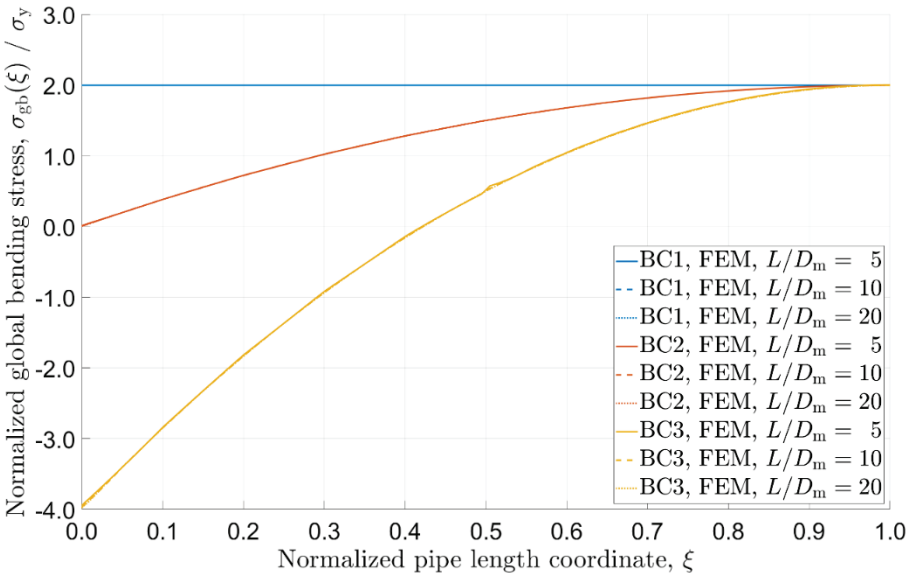

Figure 10 Normalized global bending stress versus normalized pipe length coordinate.

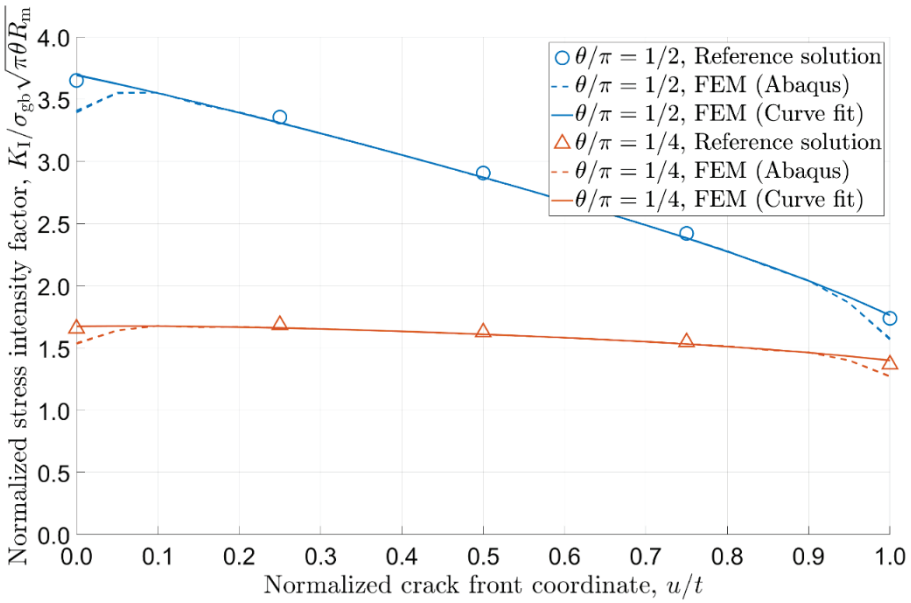

Figure 11 Normalized stress intensity factor versus normalized crack front coordinate.

2.5 R6-estimation and plasticity correction

An estimation of elastic-plastic *J*-values can be obtained from linear elastic *J*-values using the plasticity correction function in eq. (1) according to the approximate Option 2 type R6 Revision 4 failure assessment curve [18] up to Amendment 10 (at Amendment 11 it was decided to remove ρ and focus on the use of V). The global bending considered here is assumed to be a result from an entirely primary loading which means that $\rho = 0$. The correction function versus limit load parameter L_r is shown in Figure 12. The maximum allowed limit load parameter is $L_\mathrm{r}^{\max} = 1.5$.

Evaluation of the limit load parameter L_r follows the procedure outlined in [19]. Due to the absence of membrane loading, the evaluation is reduced to eq. (6). The limit load parameter versus normalized global bending stress is shown in Figure 13 for $\theta/\pi = 1/8, 1/4, 1/2$. The limit load solutions presented in [19] have been derived assuming unrestrained pipe ends. Although this report investigates the influence from different restraints, the limit load parameter L_r referred to in this report assumes unrestrained pipe ends.

$$J_{\mathrm{R6}} = J_{\mathrm{LE}} \cdot \frac{1}{[f_{\mathrm{R6}}(L_\mathrm{r}) - \rho]^2} \tag{1}$$

$$f_{\mathrm{R6}}(L_\mathrm{r}) = f_2^{\mathrm{cy}}(L_\mathrm{r}) \quad \text{Continuous yielding} \tag{2}$$

$$f_2^{\mathrm{cy}}(L_\mathrm{r}) = \begin{cases} \dfrac{0.3 + 0.7e^{-\mu L_\mathrm{r}^6}}{\sqrt{1 + 0.5L_\mathrm{r}^2}} & L_\mathrm{r} \le 1 \\ f_2^{\mathrm{cy}}(1) \cdot L_\mathrm{r}^{\frac{N_{\mathrm{R6}}-1}{2N_{\mathrm{R6}}}} & 1 < L_\mathrm{r} < L_\mathrm{r}^{\max} \end{cases} \tag{3}$$

$$\mu = \min\left(\frac{0.001\mathrm{E}}{\sigma_\mathrm{y}}, 0.6\right) \tag{4}$$

$$N_{\mathrm{R6}} = 0.3\left[1 - \frac{\sigma_\mathrm{y}}{\sigma_\mathrm{u}}\right] \tag{5}$$

$$L_\mathrm{r} = \frac{\sigma_{\mathrm{gb}}}{s_{\mathrm{gb}}} \tag{6}$$

$$s_{\mathrm{gb}} = \left(\frac{4}{\pi}\sin\beta - \frac{2}{\pi}\sin\theta\right)\sigma_\mathrm{y} \tag{7}$$

$$\beta = \frac{1}{2}(\pi - \theta) \tag{8}$$

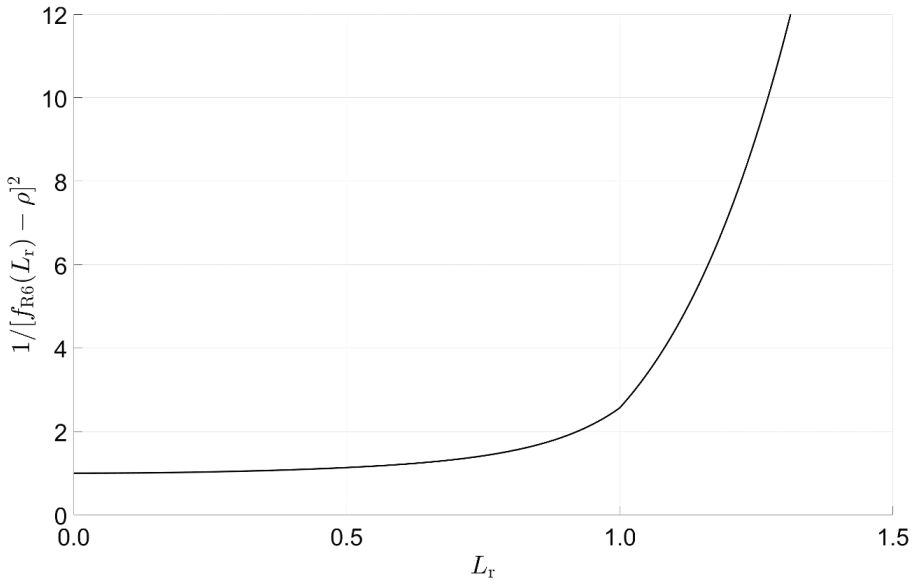

Figure 12 Plasticity correction function versus limit load parameter.

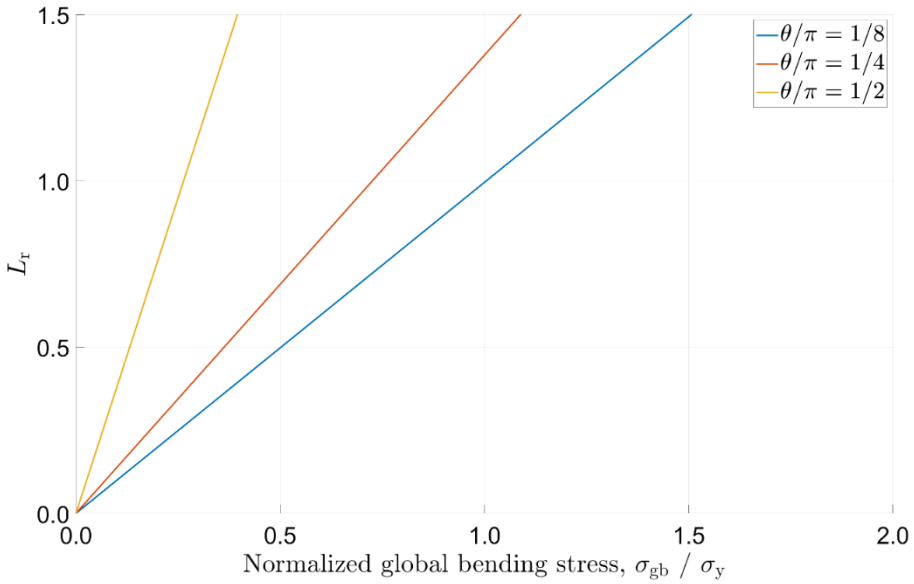

Figure 13 Limit load parameter versus normalized global bending stress.

3 RESULTS

The global nominal bending stress required to reach onset of linear elastic fracture at any of three selected locations along the crack front ($u/t = 0.0$, $u/t = 0.5$ and $u/t = 1.0$) for the reference case BC1 is presented in Table 1. The *J*-values are independent of the normalized restraint length L/D_{m}, as may be expected for BC1. For the geometries in this report, it should be noted that linear elastic fracture is initiated at the pipe inner radius for $\theta/\pi = 1/2$ and $\theta/\pi = 1/4$ while at the pipe outer radius for $\theta/\pi = 1/8$. The corresponding limit load parameter values, failure assessment curve values and plasticity correction function values at onset of linear elastic fracture for BC1 are presented in Table 2.

Normalized linear elastic and elastic-plastic *J*-values versus normalized crack front coordinates for one of the analysed cases are shown in Figure 14. The figure shows how the distribution of *J*-values along the crack front changes with increasing levels of L_{r}. The linear elastic *J*-values remain monotonic along the crack front with the consequence that onset of linear elastic fracture is obtained at either the pipe inner radius ($u/t = 0.0$) or pipe outer radius ($u/t = 1.0$). After the elastic phase, however, the elastic-plastic *J*-values increase primarily along the interior part of the crack front. This means that the maximum *J*-values move towards the interior part of the crack front, which may be explained by plasticity effects. The margin against fracture based on an elastic-plastic analysis is consequently determined by the state along the interior part of the crack front, in contrast to the R6-estimation with plastic correction of linear elastic *J*-values determined at the surface breaking points.

The present work is primarily focused on the influence from boundary restraints when assessing the margin against fracture and leakage rates. The margin against fracture increases with decreasing *J*-values whereas the leakage rate increases with increasing COD. The influence from boundary restraints has been investigated for both linear elastic *J*-values (located at either the pipe inner radius or pipe outer radius) and elastic-plastic *J*-values (located along the interior part of the crack front, from now on approximated by $u/t = 0.5$). This use of different geometrical locations is judged to be appropriate since these are the respective geometrical locations when the two approaches would be independently evaluated.

Whereas *J*-values have been extracted along the crack front, COD are here based on minimum values extracted at any of the three locations through the thickness ($u/t = 0.0$, $u/t = 0.5$ and $u/t = 1.0$) along the centre of the crack opening, corresponding to the location $\theta/\pi = 0$.

The analyses in this report show that there is a negligible difference between the boundary conditions BC1 and BC2 for both linear elastic and elastic-plastic *J*-values as well as COD. This is explained by the identical end constraints and will not be further discussed in this report. However, a significant difference between the boundary conditions BC1 and BC3 may be obtained in certain cases.

Normalized *J*-values at onset of linear elastic fracture for BC1 are presented in Table 3. Detailed information about normalized *J*-values as function of the limit load parameter L_r during the entire loading phase, until the onset of linear elastic fracture for BC1, are available in appendix A1. The corresponding results for COD are presented in Table 4 and appendix A2.

Table 1 Global nominal bending stress required to reach onset of linear elastic fracture at any location along the crack front for BC1. The load required is independent of the restraint length.

R_m [mm]	t [mm]	$\frac{\theta}{\pi}$	σ_{gb} [MPa]	$\frac{J_{LE}^{BC1}}{J_{Ic}}$		
				$\frac{u}{t}=0.0$	$\frac{u}{t}=0.5$	$\frac{u}{t}=1.0$
50	5	1/8	649	0.67	0.90	1.00
		1/4	354	1.00	0.93	0.70
		1/2	113	1.00	0.61	0.23
300	30	1/8	265	0.67	0.90	1.00
		1/4	145	1.00	0.93	0.70
		1/2	46	1.00	0.61	0.23

Table 2 Limit load parameter values, failure assessment curve values and plasticity correction function values at onset of linear elastic fracture for BC1.

R_m [mm]	t [mm]	$\frac{\theta}{\pi}$	$\frac{\sigma_{gb}}{\sigma_y}$	L_r	$f_{R6}(L_r)$	$\frac{1}{[f_{R6}(L_r)-\rho]^2}$
50	5	1/8	1.30	1.29	0.30	10.93
		1/4	0.71	0.98	0.65	2.35
		1/2	0.23	0.86	0.77	1.71
300	30	1/8	0.53	0.53	0.93	1.15
		1/4	0.29	0.40	0.96	1.08
		1/2	0.09	0.35	0.97	1.06

Table 3 Normalized *J*-values at onset of linear elastic fracture for BC1.

R_m [mm]	t [mm]	$\frac{\theta}{\pi}$	L_r	$\frac{L}{D_m}$	$\frac{J_{LE}^{BC2}}{J_{LE}^{BC1}}$	$\frac{J_{LE}^{BC3}}{J_{LE}^{BC1}}$	$\frac{J_{EP}^{BC1}}{J_{LE}^{BC1}}$	$\frac{J_{EP}^{BC2}}{J_{LE}^{BC1}}$	$\frac{J_{EP}^{BC3}}{J_{LE}^{BC1}}$	$\frac{J_{EP}^{BC2}}{J_{EP}^{BC1}}$	$\frac{J_{EP}^{BC3}}{J_{EP}^{BC1}}$
50	5	1/8	1.29	5	1.00	0.97	17.25	15.89	2.69	0.92	0.16
				10	1.00	0.98	17.26	16.90	3.75	0.98	0.22
				20	1.00	0.99	17.26	17.17	5.20	0.99	0.30
		1/4	0.98	5	1.00	0.81	2.21	2.21	1.21	1.00	0.55
				10	1.00	0.89	2.21	2.21	1.53	1.00	0.69
				20	1.00	0.94	2.21	2.21	1.79	1.00	0.81
		1/2	0.86	5	1.00	0.24	1.19	1.19	0.18	1.00	0.15
				10	1.00	0.43	1.19	1.19	0.36	1.00	0.30
				20	1.00	0.63	1.19	1.19	0.57	1.00	0.48
300	30	1/8	0.53	5	1.00	0.97	1.26	1.26	1.19	1.00	0.94
				10	1.00	0.98	1.26	1.26	1.22	1.00	0.97
				20	1.00	0.99	1.26	1.26	1.24	1.00	0.98
		1/4	0.40	5	1.00	0.81	1.24	1.24	0.94	1.00	0.76
				10	1.00	0.89	1.24	1.24	1.07	1.00	0.86
				20	1.00	0.94	1.24	1.24	1.15	1.00	0.93
		1/2	0.35	5	1.00	0.24	0.79	0.79	0.15	1.00	0.19
				10	1.00	0.43	0.79	0.79	0.29	1.00	0.37
				20	1.00	0.63	0.79	0.79	0.45	1.00	0.57

Table 4 Normalized COD-values at onset of linear elastic fracture for BC1.

R_m [mm]	t [mm]	$\frac{\theta}{\pi}$	L_r	$\frac{L}{D_m}$	$\frac{\delta_{LE}^{BC2}}{\delta_{LE}^{BC1}}$	$\frac{\delta_{LE}^{BC3}}{\delta_{LE}^{BC1}}$	$\frac{\delta_{EP}^{BC1}}{\delta_{LE}^{BC1}}$	$\frac{\delta_{EP}^{BC2}}{\delta_{LE}^{BC1}}$	$\frac{\delta_{EP}^{BC3}}{\delta_{LE}^{BC1}}$	$\frac{\delta_{EP}^{BC2}}{\delta_{EP}^{BC1}}$	$\frac{\delta_{EP}^{BC3}}{\delta_{EP}^{BC1}}$
50	5	1/8	1.29	5	1.00	0.98	18.37	16.98	3.40	0.92	0.19
				10	1.00	0.99	18.39	18.02	4.64	0.98	0.25
				20	1.00	0.99	18.39	18.29	6.26	0.99	0.34
		1/4	0.98	5	1.00	0.90	2.22	2.22	1.40	1.00	0.63
				10	1.00	0.95	2.22	2.22	1.67	1.00	0.75
				20	1.00	0.97	2.22	2.22	1.88	1.00	0.85
		1/2	0.86	5	1.00	0.49	1.50	1.50	0.51	1.00	0.34
				10	1.00	0.66	1.50	1.50	0.73	1.00	0.49
				20	1.00	0.79	1.50	1.50	0.95	1.00	0.63
300	30	1/8	0.53	5	1.00	0.98	1.19	1.18	1.15	0.99	0.97
				10	1.00	0.99	1.19	1.19	1.16	1.00	0.97
				20	1.00	0.99	1.19	1.19	1.17	1.00	0.98
		1/4	0.40	5	1.00	0.90	1.12	1.12	0.97	1.00	0.87
				10	1.00	0.95	1.12	1.12	1.03	1.00	0.92
				20	1.00	0.97	1.12	1.12	1.07	1.00	0.96
		1/2	0.35	5	1.00	0.49	1.06	1.06	0.49	1.00	0.46
				10	1.00	0.66	1.06	1.06	0.67	1.00	0.63
				20	1.00	0.79	1.06	1.06	0.81	1.00	0.76

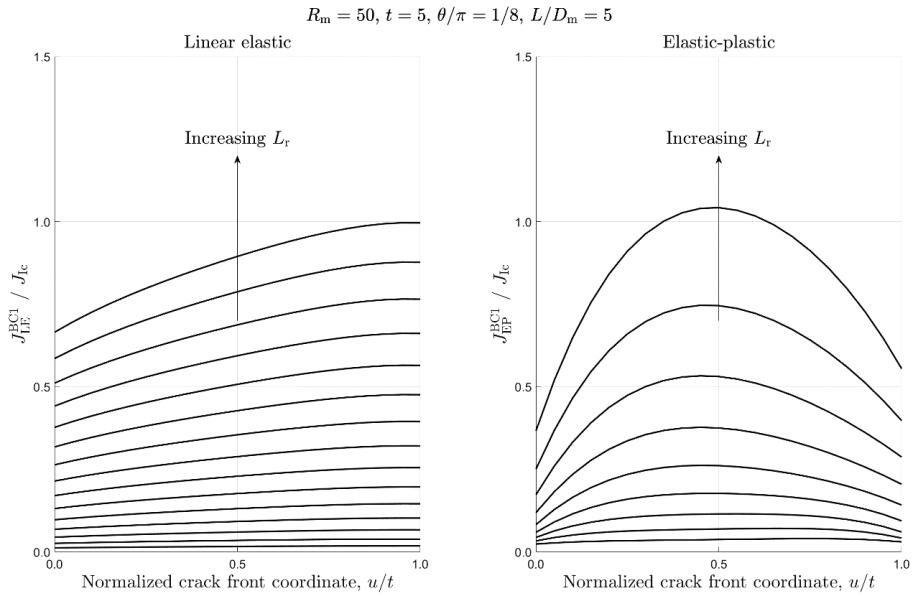

Figure 14 Normalized linear elastic and elastic-plastic J-values versus normalized crack front coordinates with increasing levels of L_r.

4 CONCLUSIONS

The main conclusions are:

- The linear elastic as well as elastic-plastic *J*-values have been shown to vary significantly along the analysed crack fronts. It may be necessary to discuss the applicability and relevance of idealised TWCs.

- The elastic-plastic *J*-values increase primarily along the interior part of the crack front after the elastic phase. The margin against fracture based on an elastic-plastic analysis is therefore determined by the state along the interior part of the crack front, in contrast to the R6-estimation with plastic correction of linear elastic *J*-values determined at the surface breaking points.

- Comparison between cases with identical end constraint but different loading origins reveals a negligible difference in results. The end constraints are more important than the load origin itself for the cases studied here. This may be significant for other cases where global bending stress is present, independent of the origin for moment loading, e.g. dead weight, internal pressure or a combination of loads.

- Linear elastic *J*-values are independent of restraint length for BC1, but dependent of restraint length for BC3. Both linear elastic and elastic-plastic *J*-values are consistently lower for BC3 for all analysed cases. The relative difference in linear elastic *J*-values between BC3 and BC1 increases with decreasing restraint length and/or increasing relative crack length. Although the limit load parameter is influenced, the relative difference in linear elastic *J*-values between BC3 and BC1 is independent of pipe dimension. A similar trend, although more pronounced, can be observed for elastic-plastic *J*-values.

- The results show that the R6-method is in good agreement with the elastic-plastic *J*-values for the cases studied in this report. Differences in the results should be observed primarily with respect to the limit load parameter L_{r} which is the dimensioning factor. The R6-estimate is slightly non-conservative relative the elastic-plastic values for both BC1 and BC3 for the smallest relative crack length ($\theta/\pi = 1/8$). For the medium relative crack length ($\theta/\pi = 1/4$), the R6-estimate is conservative relative the elastic-plastic values for BC3, and slightly non-conservative relative the elastic-plastic values for BC1. The R6-estimate is entirely conservative for the largest relative crack length ($\theta/\pi = 1/2$).

- The results for COD are influenced by restraint length, relative crack length, degree of restraint and material constitutive properties in the same way as the *J*-values. However, the relative difference was generally smaller for the COD. The COD values and subsequently the leak rates may be overestimated in LBB assessments if pipe end restraints are not carefully considered.

- It is recommended that the influence from restraint is studied in detail as an LBB assessment of a selected case based on a real piping system analysis. The results from a detailed simulation of loadings and structural stiffness should be compared with the results obtained from common practice methods. Reliable conclusions can only be drawn taking the margin against fracture, leak detection as well as degradation mechanisms into account.

5 REFERENCES

[1] R. Bourga, P. Moore, Y.-J. Janin, B. Wang and J. Sharples, "Leak-before-break: Global perspectives and procedures," *International Journal of Pressure Vessels and Piping,* Vols. 129-130, pp. 43-49, 2015.

[2] G. Wilkowski, R. Schmidt, P. Scott, R. Olson, C. Marschall, G. Kramer and D. Paul, "International Piping Integrity Research Group (IPIRG) Program - Program Final Report," NUREG/CR-6233, 1997.

[3] G. Wilkowski, B. Brust, T. Zhang, G. Hattery, S. Kalyanam, D.-J. Shim, E. Kurth, Y. Hioe, M. Uddin, J. J. Johnson, O. R. Maslenikov, A. Gürpinar, A. P. Asfura, B. Sumodobila, A. A. Betervide and O. Mazzantini, "Robust LBB Analyses for Atucha II Nuclear Plant," in *ASME 2011 Pressure Vessels and Piping Conference*, Baltimore, 2011.

[4] N. Ghadiali, S. Rahman, Y. H. Choi and G. Wilkowski, "Deterministic and Probabilistic Evaluations for Uncertainty in Pipe Fracture Parameters in Leak-Before-Break and In-Service Flaw Evaluations," NUREG/CR-6443, 1996.

[5] S. Rahman, F. Brust, N. Ghadiali, Y. H. Choi, P. Krishnaswamy, F. Moberg, B. Brickstad and G. Wilkowski, "Refinement and Evaluation of Crack-Opening-Area Analyses for Circumferential Through-Wall Cracks in Pipes," NUREG/CR-6300, 1995.

[6] P. M. Scott, R. J. Olson and G. M. Wilkowski, "Development of Technical Basis for Leak-Before-Break Evaluation Procedures," NUREG/CR-6765, 2002.

[7] P. Scott, R. Olson, J. Bockbrader, M. Wilson, B. Gruen, R. Morbitzer, Y. Yang, C. Williams, F. Burst, L. Fredette, N. Ghadiali, G. Wilkowski, D. Rudland, Z. Feng and R. Wolterman, "The Batelle Integrity of Nuclear Piping (BINP) Program Final Report - Summary and Implications of Results," NUREG/CR-6837, 2005.

[8] J.-W. Kim, "Evaluation of restraint effect of pressure induced bending on the elastic-plastic crack opening behaviour," *International Journal of Pressure Vessels and Piping,* vol. 81, no. 4, pp. 335-362, 2004.

[9] B. Brickstad, "Rörbrottskydd och läckage före brott (LBB)," SKI 2005/83, Stockholm, 2005.

[10] R. Olson, R. A. Morbitzer, P. M. Scott och G. M. Wilkowski, ”Practical Application of Restraint of Pressure-Induced Bending Phenomenon in Leak Rate Calculations,” i *SMiRT 17*, Prague, 2003.

[11] B. A. Young och R. J. Olson, ”System Stiffness and Restraint Effects on Circumferential Crack Opening Displacement - A

Rotational Approach," i *ASME 2015 Pressure Vessels and Piping*, Boston, 2015.

[12] J.-W. Kim, "Evaluation Model for Restraint Effect of Pressure Induced Bending on the Plastic Crack Opening of a Circumferential Through Wall Crack," *Nuclear Engineering and Technology,* vol. 39, nr 1, pp. 75-84, 2007.

[13] J.-W. Kim, "A practical application of an evaluation model for the restraint effect of pressure-induced bending on a plastic crack opening," *International Journal of Pressure Vessels and Piping,* vol. 85, nr 8, pp. 557-568, 2008.

[14] Y. Kim, I.-S. Hwang och Y.-J. Oh, "Effective applied moment in circumferential through-wall cracked pipes for leak-before-break evaluation considering pipe restraint effects," *Nuclear Engineering and Design,* vol. 301, pp. 175-182, 2016.

[15] Y. Kim, Y.-J. Oh och H.-B. Park, "The Conservatism of Leak Before Break Analysis in Terms Of The Applied Moment At Cracked Section," i *ASME 2016 Pressure Vessels and Piping*, Vancouver, 2016.

[16] Abaqus R2018, Dassault Systèmes.

[17] W. Zang, "Stress intensity factor solutions for axial and circumferential through-wall cracks in cylinders," SINTAP/SAQ/02, 1997.

[18] "Assessment of the integrity of structures containing defects, R6 Rev. 4, Up to amendment record No.10," EDF Energy Nuclear Generation Ltd., 2013.

[19] P. Delfin, "Limit load solutions for cylinders with circumferential cracks subjected to tension and bending," SAQ/FoU-Report 96/05, 1996.

A1 NORMALIZED *J*-VALUES VS. L_r

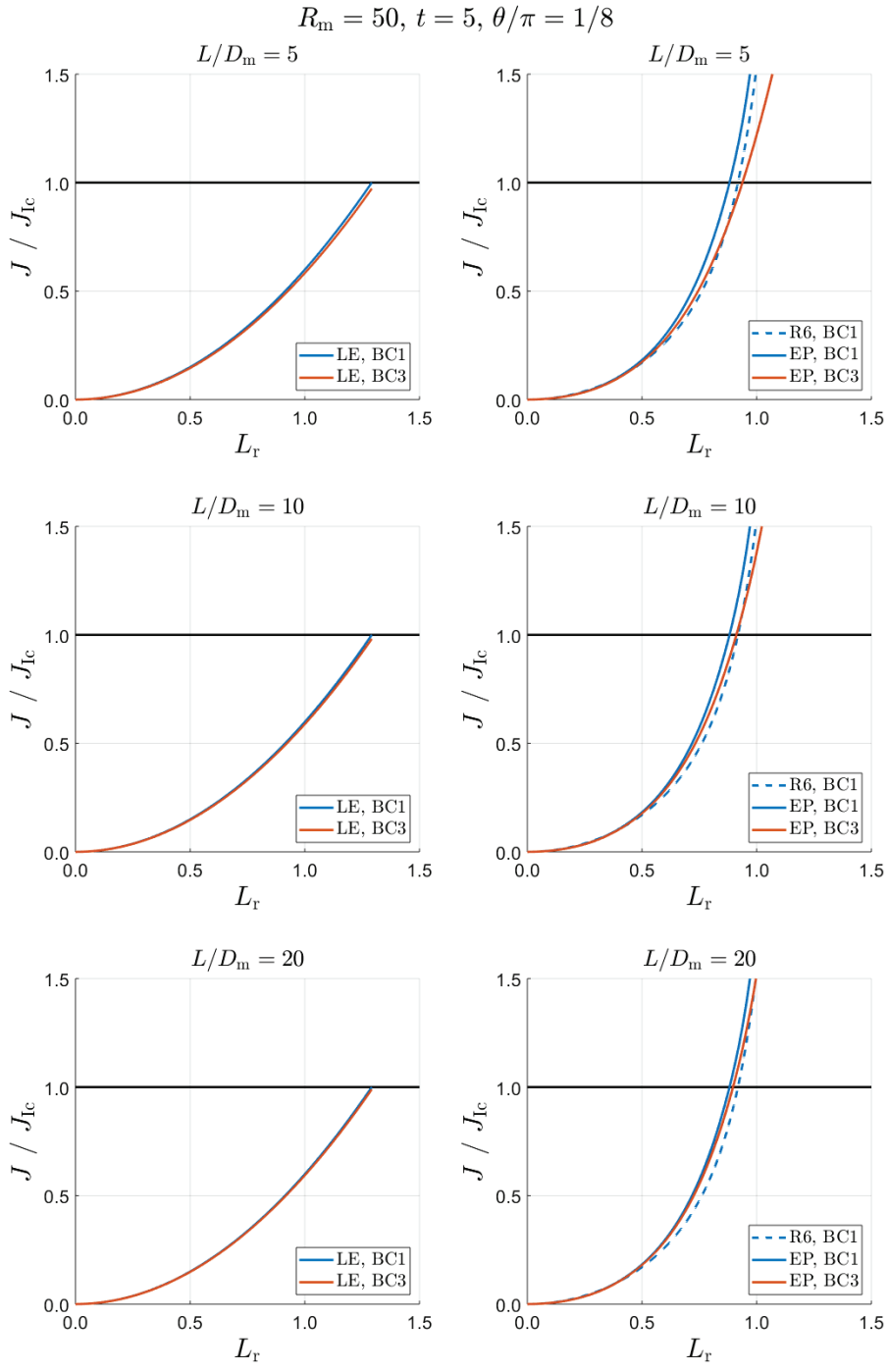

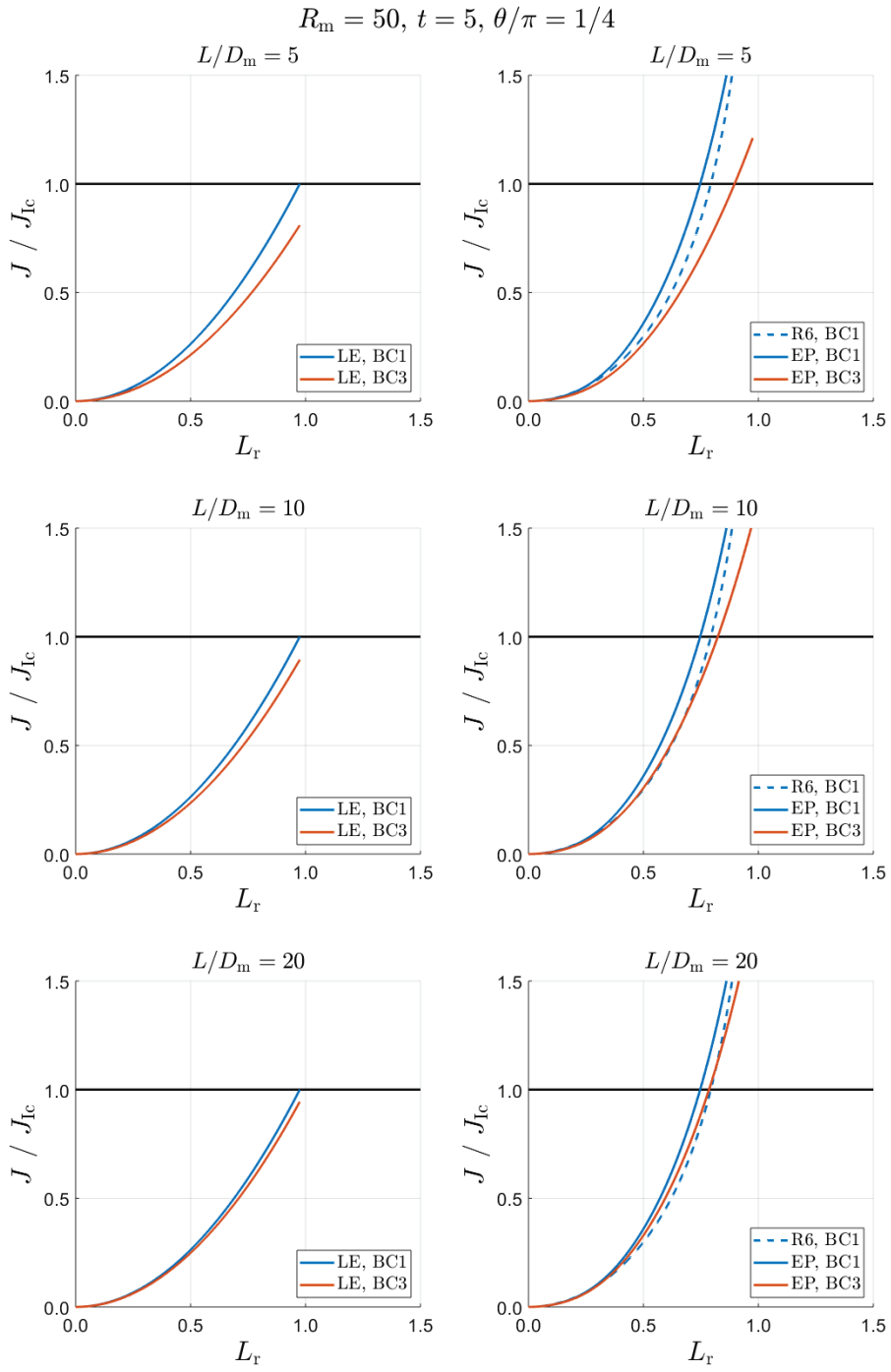
$R_m = 50,\ t = 5,\ \theta/\pi = 1/4$
$L/D_m = 5$
$L/D_m = 5$
$L/D_m = 10$
$L/D_m = 10$
$L/D_m = 20$
$L/D_m = 20$
$J\ /\ J_{Ic}$
L_r
LE, BC1
LE, BC3
R6, BC1
EP, BC1
EP, BC3
0.0
0.5
1.0
1.5

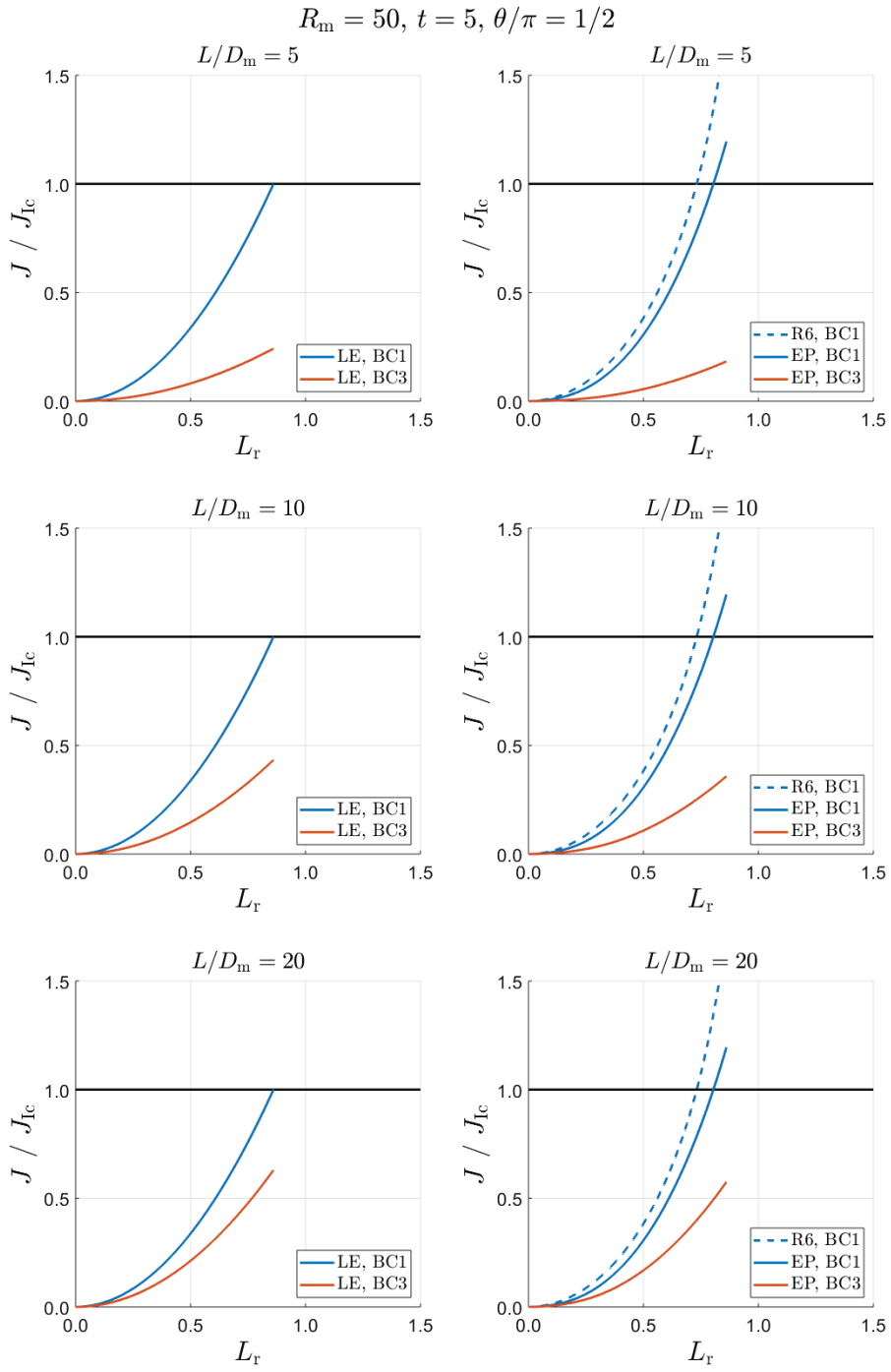
$R_m = 50,\ t = 5,\ \theta/\pi = 1/2$
$L/D_m = 5$
$L/D_m = 5$
$L/D_m = 10$
$L/D_m = 10$
$L/D_m = 20$
$L/D_m = 20$
$J\ /\ J_{Ic}$
L_r
LE, BC1
LE, BC3
R6, BC1
EP, BC1
EP, BC3
0.0
0.5
1.0
1.5

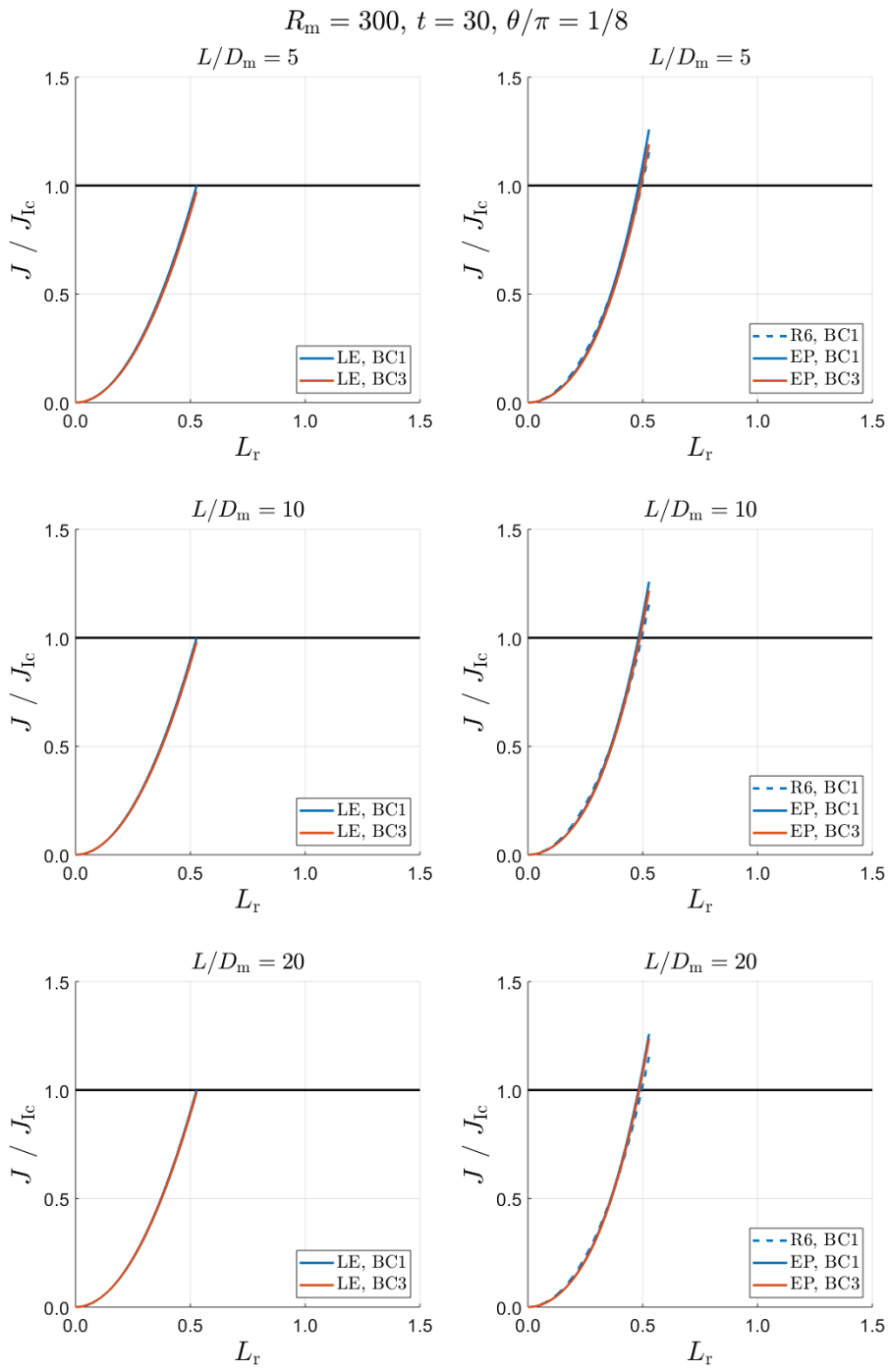
$R_{\mathrm{m}} = 300,\ t = 30,\ \theta/\pi = 1/8$
$L/D_{\mathrm{m}} = 5$
$L/D_{\mathrm{m}} = 5$
$L/D_{\mathrm{m}} = 10$
$L/D_{\mathrm{m}} = 10$
$L/D_{\mathrm{m}} = 20$
$L/D_{\mathrm{m}} = 20$
$J\ /\ J_{\mathrm{Ic}}$
L_{r}
0.0
0.5
1.0
1.5
LE, BC1
LE, BC3
R6, BC1
EP, BC1
EP, BC3

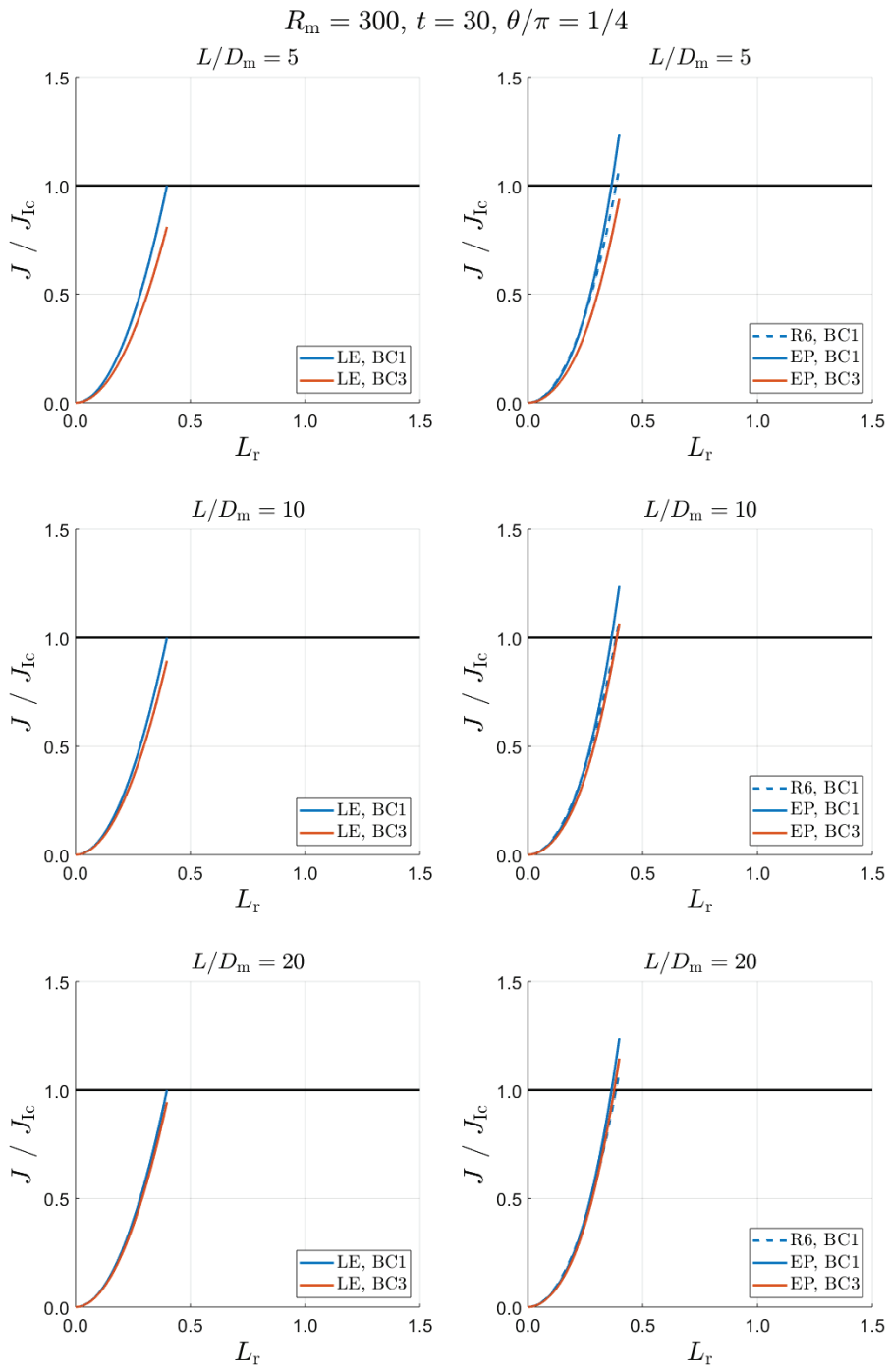
$R_{\mathrm{m}} = 300,\ t = 30,\ \theta/\pi = 1/4$
$L/D_{\mathrm{m}} = 5$
$L/D_{\mathrm{m}} = 5$
$L/D_{\mathrm{m}} = 10$
$L/D_{\mathrm{m}} = 10$
$L/D_{\mathrm{m}} = 20$
$L/D_{\mathrm{m}} = 20$
$J\ /\ J_{\mathrm{Ic}}$
L_{r}
0.0
0.5
1.0
1.5
LE, BC1
LE, BC3
R6, BC1
EP, BC1
EP, BC3

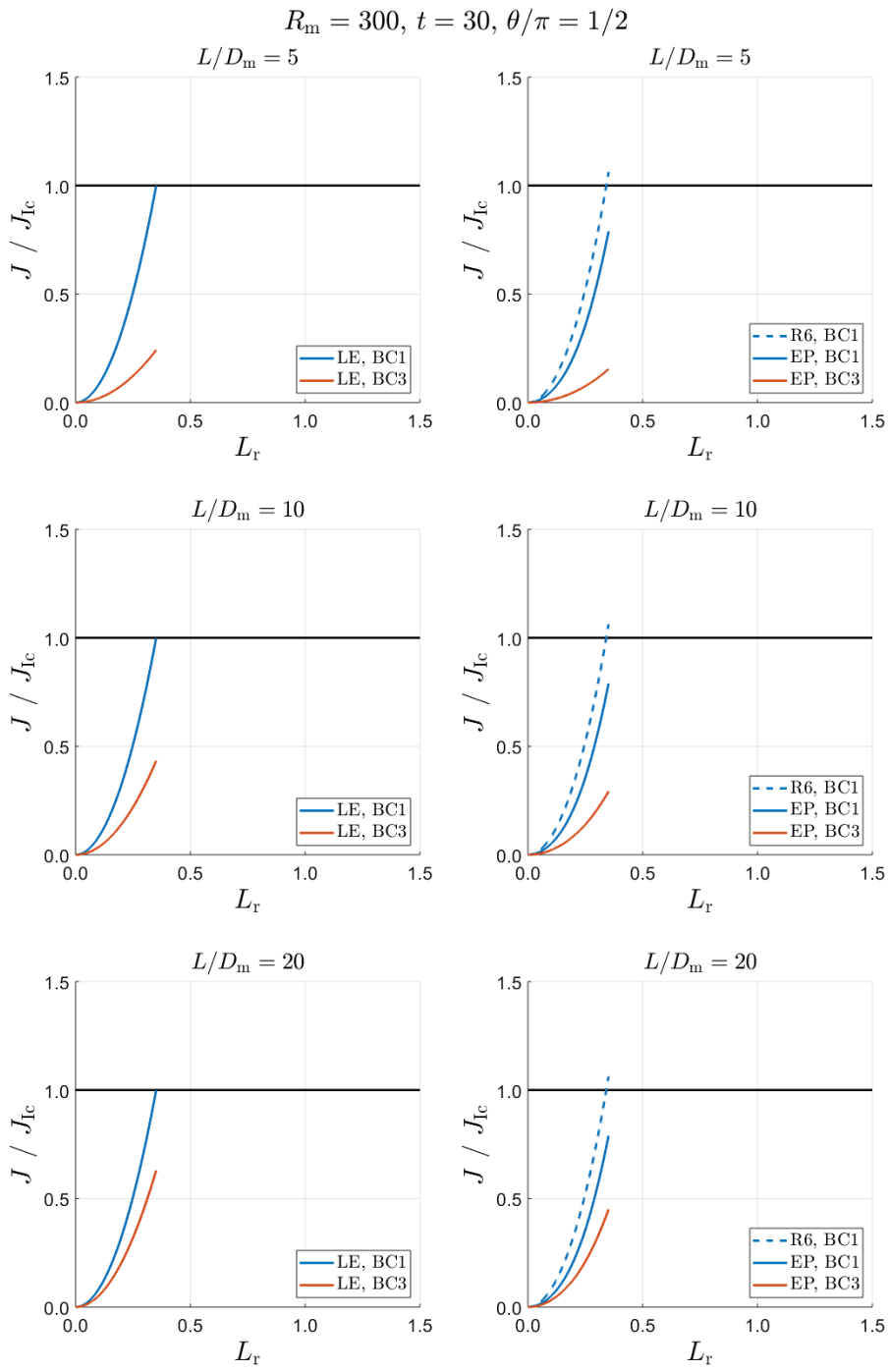
$R_{\mathrm{m}} = 300,\ t = 30,\ \theta/\pi = 1/2$
$L/D_{\mathrm{m}} = 5$
$L/D_{\mathrm{m}} = 5$
$L/D_{\mathrm{m}} = 10$
$L/D_{\mathrm{m}} = 10$
$L/D_{\mathrm{m}} = 20$
$L/D_{\mathrm{m}} = 20$
$J\ /\ J_{\mathrm{Ic}}$
L_{r}
LE, BC1
LE, BC3
R6, BC1
EP, BC1
EP, BC3
0.0
0.5
1.0
1.5

A2 NORMALIZED COD VS. L_r

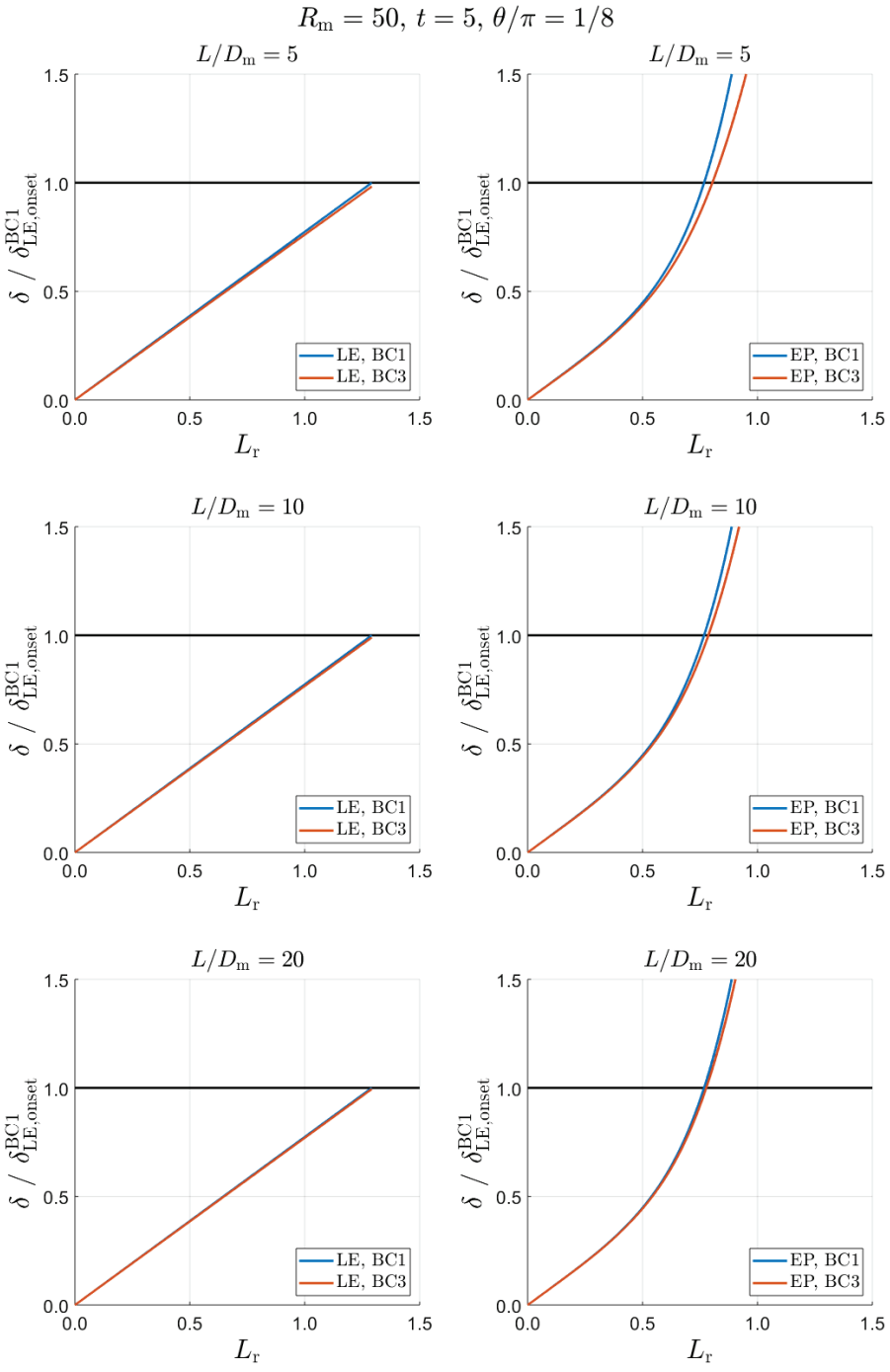

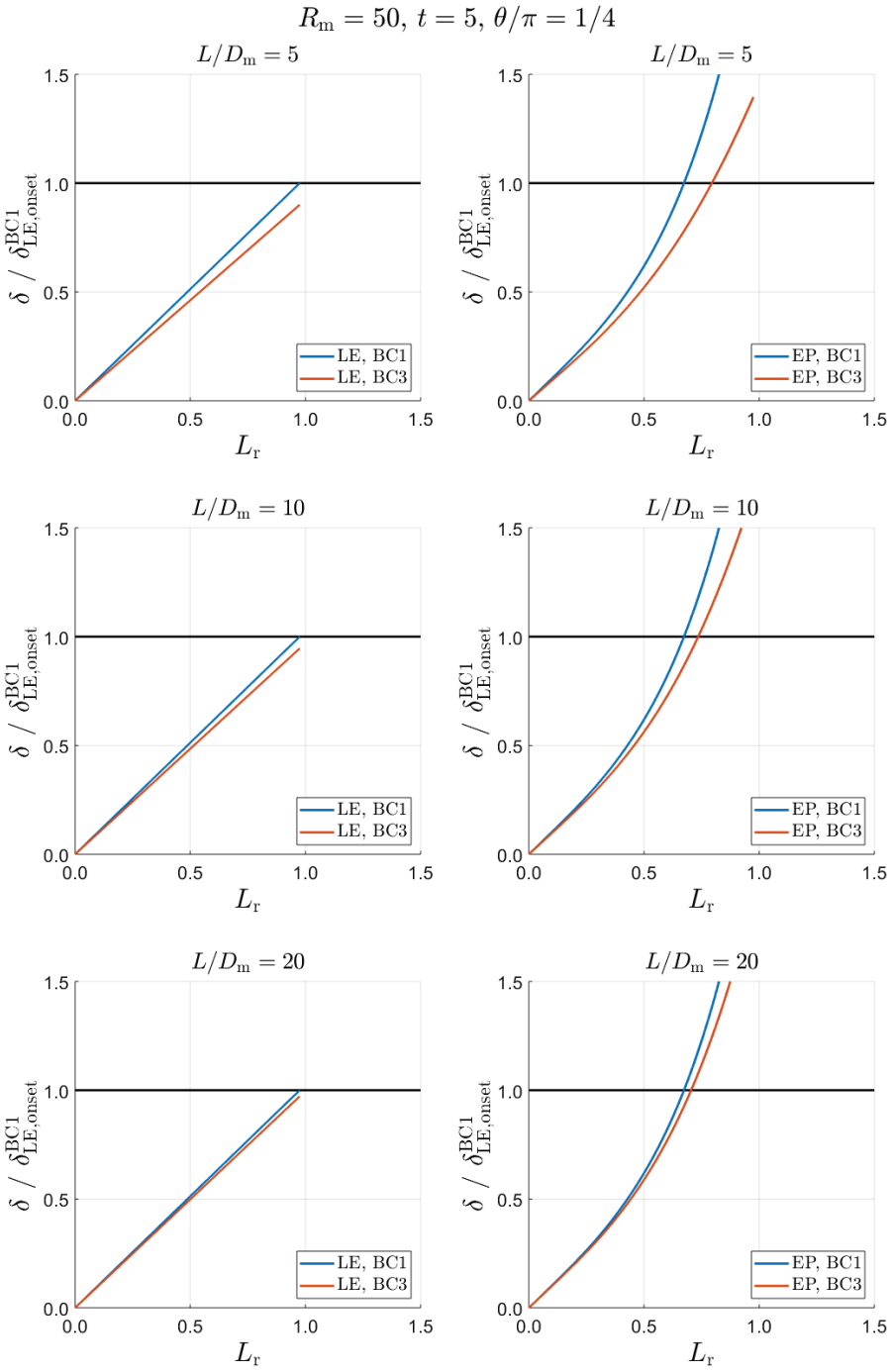
$R_\mathrm{m} = 50,\ t = 5,\ \theta/\pi = 1/4$
$L/D_\mathrm{m} = 5$
$L/D_\mathrm{m} = 5$
$L/D_\mathrm{m} = 10$
$L/D_\mathrm{m} = 10$
$L/D_\mathrm{m} = 20$
$L/D_\mathrm{m} = 20$
$\delta\ /\ \delta^{\mathrm{BC1}}_{\mathrm{LE,onset}}$
L_r
LE, BC1
LE, BC3
EP, BC1
EP, BC3
0.0
0.5
1.0
1.5

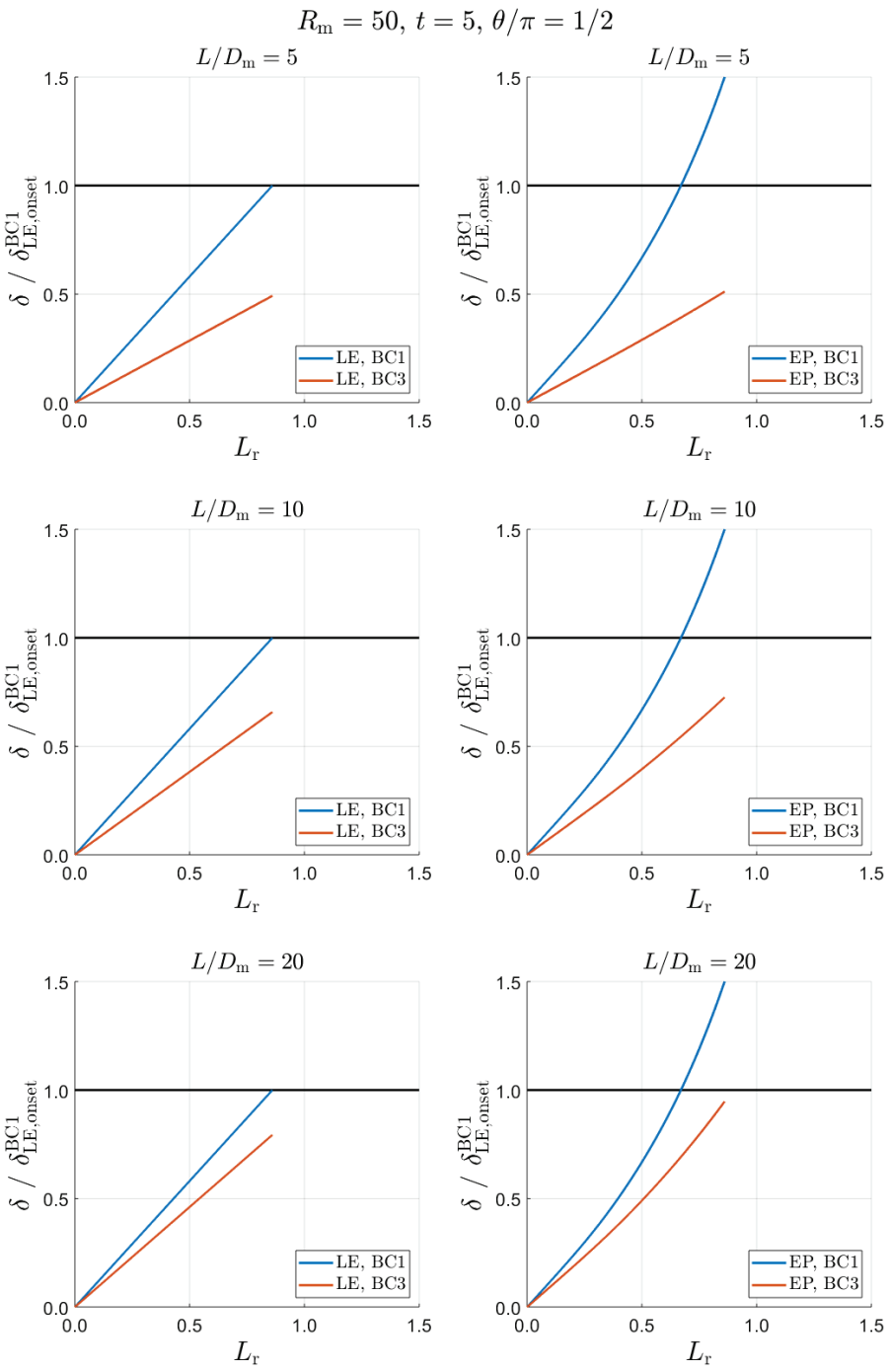
$R_\mathrm{m} = 50,\ t = 5,\ \theta/\pi = 1/2$
$L/D_\mathrm{m} = 5$
$L/D_\mathrm{m} = 5$
$L/D_\mathrm{m} = 10$
$L/D_\mathrm{m} = 10$
$L/D_\mathrm{m} = 20$
$L/D_\mathrm{m} = 20$
$\delta\ /\ \delta^{\mathrm{BC1}}_{\mathrm{LE,onset}}$
L_r
LE, BC1
LE, BC3
EP, BC1
EP, BC3
0.0
0.5
1.0
1.5

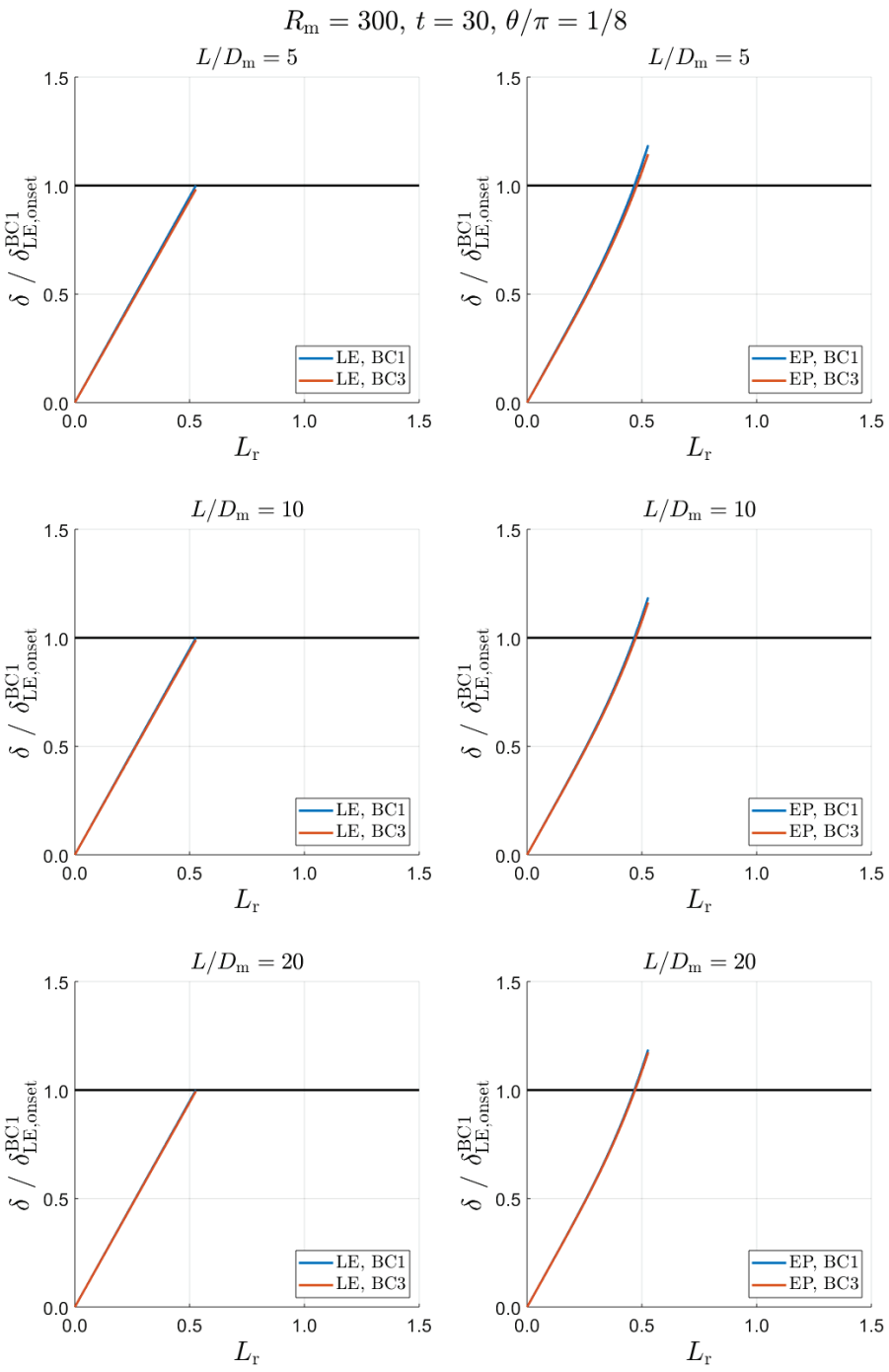
$R_\mathrm{m} = 300,\ t = 30,\ \theta/\pi = 1/8$
$L/D_\mathrm{m} = 5$
$L/D_\mathrm{m} = 5$
$L/D_\mathrm{m} = 10$
$L/D_\mathrm{m} = 10$
$L/D_\mathrm{m} = 20$
$L/D_\mathrm{m} = 20$
$\delta\ /\ \delta^{\mathrm{BC1}}_{\mathrm{LE,onset}}$
L_r
LE, BC1
LE, BC3
EP, BC1
EP, BC3
0.0
0.5
1.0
1.5

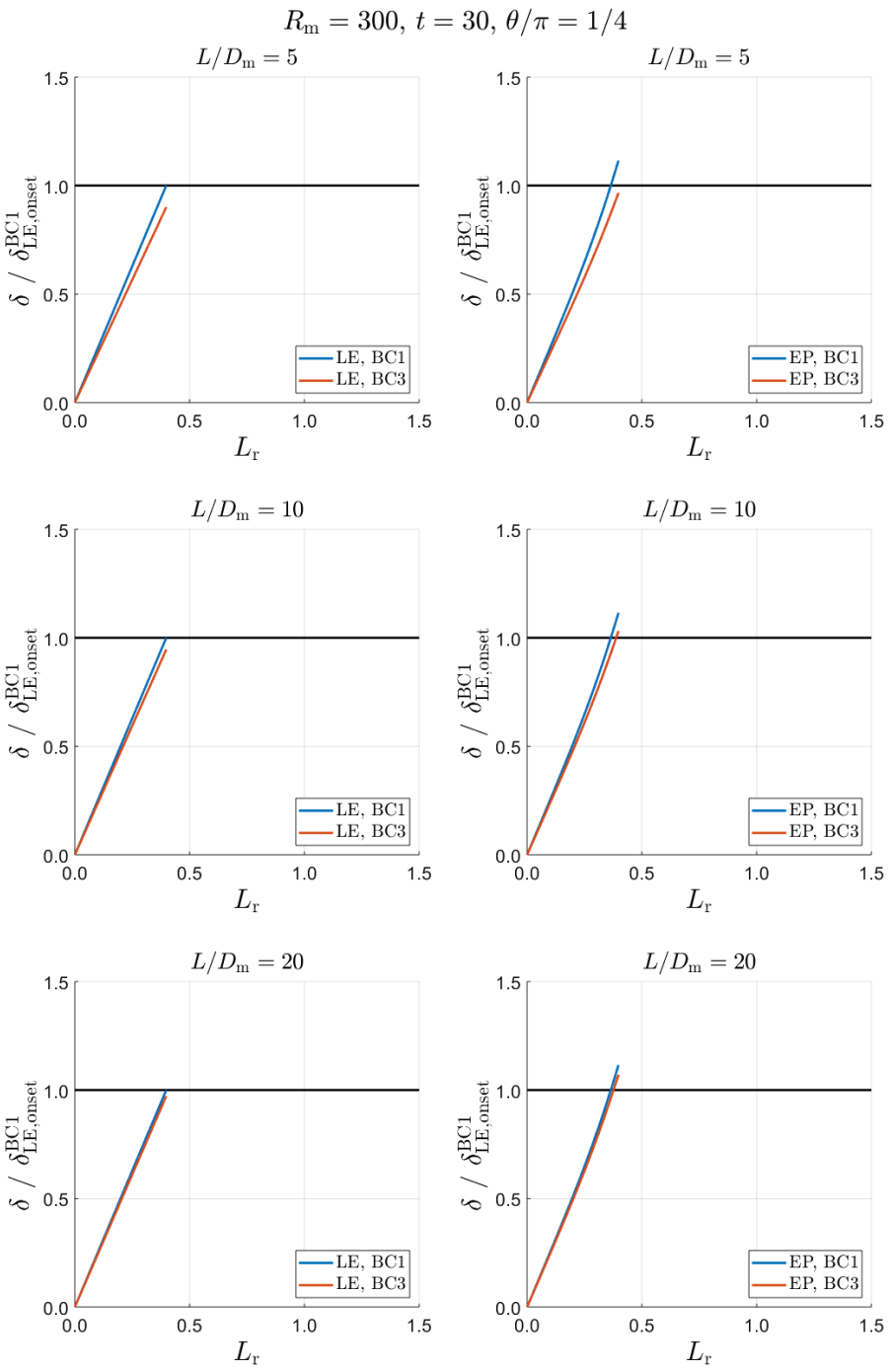
$R_\mathrm{m} = 300,\ t = 30,\ \theta/\pi = 1/4$
$L/D_\mathrm{m} = 5$
$L/D_\mathrm{m} = 5$
$L/D_\mathrm{m} = 10$
$L/D_\mathrm{m} = 10$
$L/D_\mathrm{m} = 20$
$L/D_\mathrm{m} = 20$
$\delta\ /\ \delta^{\mathrm{BC1}}_{\mathrm{LE,onset}}$
L_r
LE, BC1
LE, BC3
EP, BC1
EP, BC3
0.0
0.5
1.0
1.5

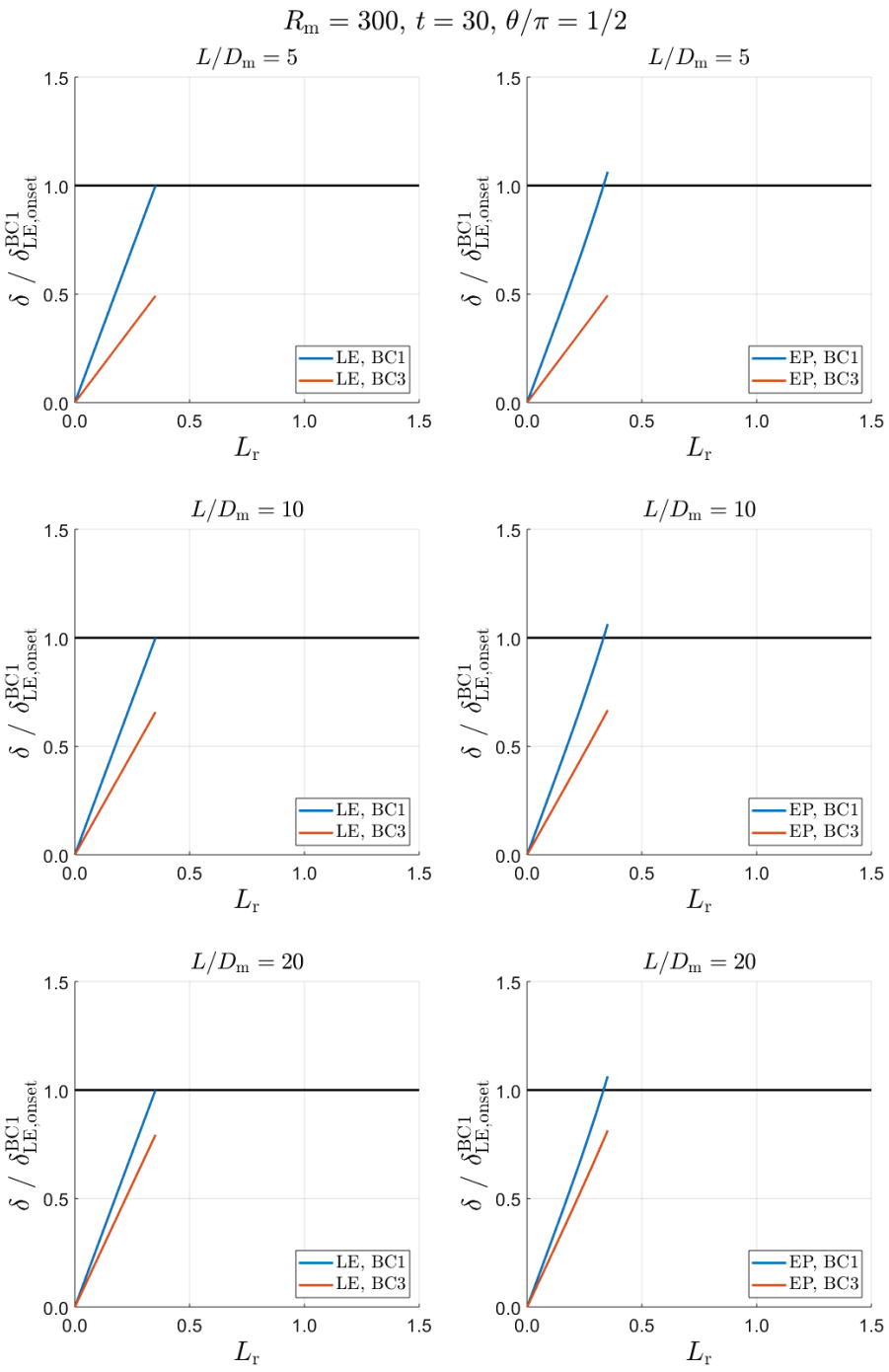
$R_\mathrm{m} = 300,\ t = 30,\ \theta/\pi = 1/2$
$L/D_\mathrm{m} = 5$
$L/D_\mathrm{m} = 5$
$L/D_\mathrm{m} = 10$
$L/D_\mathrm{m} = 10$
$L/D_\mathrm{m} = 20$
$L/D_\mathrm{m} = 20$
$\delta\ /\ \delta^{\mathrm{BC1}}_{\mathrm{LE,onset}}$
L_r
LE, BC1
LE, BC3
EP, BC1
EP, BC3
0.0
0.5
1.0
1.5

The Swedish Radiation Safety Authority has a comprehensive responsibility to ensure that society is safe from the effects of radiation. The Authority works from the effects of radiation. The Authority works to achieve radiation safety in a number of areas: nuclear power, medical care as well as commercial products and services. The Authority also works to achieve protection from natural radiation an to increase the level of ratiation safety internationally.

The Swedish Radiation Safety Authority works proactively and presentively to protect people and the environment from the harmful effects of radiation, now and in the future.
The Authority issues regulations and supervises compliance, while also supporting research, providing training and information, and issuing advice. Often, activities involving radiation require licences issued by the Authority. The Swedish Radiation Safety Authority maintains emergency preparedness around the clock with the aim of limiting the aftermath of radiation accidents and the unintentional spreading of radioactive substances. The Authority participates in international co-operation in order to promote radiation safety and finances projects aiming to raise the level of radiation safety in certain Eastern European countries.

The Authority reports to the Ministry of the Environment and has around 300 employees with competencies in the fields of engineering, natural and behavioral sciences, law, economics and communications. We have recieved quality, environmental and working environment certification.

Publikationer utgivna av Strålsäkerhetsmyndigheten kan laddas ned via stralsäkerhetsmyndigheten.se eller beställas genom att skicka e-post till registrator@ssm.se om du vill ha broschyren i alternativt format, som punktskrift eller daisy.

Strålsäkerhetsmyndigheten
Swedish Radiation Safety Authority
SE-171 16 Stockholm
Phone: 08-799 40 00
Web: ssm.se
E-mail: registrator@ssm.se

E-print AB, 2020